A Simplified Model for the On-Line Identification of Bearing Direct-Dynamic Parameters Based on Algebraic Identification (AI)

Saulo Jesús Landa-Damas [1], Jorge Colín-Ocampo [1,*], Andrés Blanco-Ortega [1], Arturo Abúndez-Pliego [1], José Gabriel Mendoza-Larios [2], Luis Alberto Baltazar-Tadeo [3] and Demetrio Pérez-Vigueras [1]

[1] Departamento de Ingeniería Mecánica, Tecnológico Nacional de México/CENIDET, Cuernavaca 62490, Morelos, Mexico; saulojesuslanda@cenidet.edu.mx (S.J.L.-D.); andres.bo@cenidet.tecnm.mx (A.B.-O.); arturo.ap@cenidet.tecnm.mx (A.A.-P.); demetrioperez16m@cenidet.edu.mx (D.P.-V.)
[2] Instituto de Ingeniería Industrial y Automotriz, Universidad Tecnológica de la Mixteca, Huajuapan de León 69000, Oaxaca, Mexico; jgml@mixteco.utm.mx
[3] UPIIP/Instituto Politécnico Nacional, Palenque 29960, Chiapas, Mexico; lbaltazart@ipn.mx
* Correspondence: jorge.co@cenidet.tecnm.mx; Tel.: +52-77-7564-8187

Abstract: In this paper, a mathematical model is presented to identify the direct dynamic coefficients (k_{xx}, k_{zz}, c_{xx}, c_{zz}) of a pressurized bearing in a rotor-bearing system. The presented mathematical model for online identification is the result of the application of the algebraic identification approach to a two-degree-of-freedom rotor-bearing model. The proposed identification model requires only the vibration response as the input data. The performance of the model was assessed by theoretically and experimentally testing the proposed identifier at different shaft frequencies and, for the experimental test, a pressurized bearing that has hydrodynamic and hydrostatic characteristics at a support pressure of 10 psi was considered. The working fluid is Chevron GST 32 oil. The results show negligible differences between the vibration response of the experimental rotor and those obtained numerically using the identified direct dynamic coefficients of the pressurized bearing. In addition, it is observed that the algebraic identifier determines the identified parameters in a time less than 0.2 s. The proposed identifier can be used in other types of bearings, which is a great advantage over other identifiers.

1. Introduction

As a rotary system supported by hydrodynamic bearings operates, pressure distribution in the oil lubricant film of the bearing is generated, which bears the rotor weight as well as the unbalanced forces acting on the rotor and directly influences the dynamic behavior of the rotor (system stability, bending critical speed, vibration modes, etc.). The bearing behavior is influenced by the magnitude of the hydrodynamic forces, which can be expressed as a function of the rotor dynamic coefficients. According to Lund [1], Vance [2], and Dimarogonas [3], there are four rotor dynamic coefficients of a bearing that represent the stiffness (k_{xx}, k_{xz}, k_{zx}, k_{zz}) and four others that represent the damping (c_{xx}, c_{xz}, c_{zx}, c_{zz}). The rotor dynamic coefficients of the fluid film in hydrodynamic bearings are calculated by analytical, numerical, and experimental approaches. Among the researchers specializing in this field, most experimentally estimate the rotor dynamic coefficients, specifically by using the response to the unbalance of the system due to the residual unbalance is always present in the rotary systems, which prevents the use of external equipment for exciting

the system. Wengui Mao et al. [4] presented an inverse method aimed at the identification of the rotor dynamic coefficients of a sliding rotor-bearing system with unbalance parameters, which consisted of the application of a dynamic-loading identification method along with the analysis of intervals. The identification of the dynamic parameters of the bearing could be formulated as the reconstruction of the force on the oil film with the experimental unbalance response. On the other hand, Changmin Chen et al. [5] proposed a novel method to avoid ill-posed problems of the coefficient identification of circular journal bearings based on the unbalance response; focused on avoiding the ill-conditioned matrix problem, they proposed four complementary equations that are independent of the dynamic equations derived from the response to the unbalance. Two equations for the damping are derived from the Reynolds equation, and two others for the stiffness are derived from the Taylor expansion of the static forces acting on the bearing. With these four equations, the identification matrix has a low condition number, which allows for a more stable and reliable parameter identification.

Machinery, in general, plays a very important role in the industry; currently, different studies have been carried out on new methodologies for the diagnosis of failures in industrial machinery [6,7]. Recently Ke Zhao et al. [8] designed a new transfer-learning framework called CWTWAE to solve the problem of rolling-bearing failure diagnosis with multi-source domains. There is vast information about rolling bearing, journal bearing and identification methods of unbalance and bearing dynamic parameters [9,10]. Colín Ocampo J. et al. [11] proposed a methodology for the angular position identification of the unbalance force based on a two-degrees-of-freedom mathematical simplified model of a rotor with unequal principal moments of inertia of the shaft transverse section. They submitted this methodology in a numerical and experimental way, obtaining encouraging results. In addition, Jianfei Yao et al. [12] proposed an integrated modal expansion/inverse problem methodology combined with an optimization procedure. This technique allowed for the identification of the axial location of the unbalance as well as its magnitude and phase. This technique was validated experimentally with acceptable error percentages. Lei Li et al. [13] used a scale model and scale laws to identify unbalance for a full-size rotor system. They tested the proposed methodology numerically and experimentally, concluding that it is feasible to identify the unbalance values of the rotor with the proposed method. Recently, Aiming Wang [14] presented the development of algorithms for the simultaneous identification of the unbalance and the bearing dynamic parameters; in both cases, the proposed algorithms were validated with experimental results. Seung Yoon On et al. [15] developed a composite tilting-pad journal bearing using a hybrid pad structure composed of a carbon fiber/epoxy composite liner and backup metal to enhance the dynamic characteristics of the bearing system. The stiffness and damping parameters of the bearing fluid film were determined by a thermohydrodynamic analysis of lubrication using the finite difference method.

In the same way, investigations have also been carried out to identify the dynamic parameters of active magnetic bearings (AMBs) in a flexible rotor system. The AMBs support rotors using electromagnetic force rather than mechanical forces [16,17]. M. Asadi Varnusfaderani et al. [18] developed an algorithm for identifying the parameters of flexible rotor systems equipped with smart magneto-rheological bearings. For the implementation of the identification algorithm, the finite element model of a flexible rotor system was equipped with magnetorheological squeeze-film dampers (MRSFDs). Eliott Guenat and Jürg Schiffmann [19] built a test rig to experimentally identify the stiffness and damping coefficients of the Herringbone Grooved Journal Bearings (HGJBs) of a rotor perturbed by piezo-electric shakers; they concluded that the Narrow Groove Theory (NGT) tends to overestimate the stiffness and damping of the HGJB. At the rated speed, direct stiffness values and damping ratios were measured to be 38% and 27% lower, respectively, than the NGT prediction.

The stiffness and damping parameters of the fluid film bearings change with the speed of the rotor, the viscosity provided by the type of oil used, pressure changes, and tempera-

ture changes, among other factors. Muhammad Imran Sadiq et al. [20] evaluated bio-oils and mineral-based oils in terms of their stiffness and damping coefficients for bearing applications. The approach they used was analytical and experimental. Rotodynamic coefficients are determined with analytical expressions that are a function of the eccentricity ratio, which is determined using the dynamic viscosity of the oil. This viscosity is obtained experimentally for different temperatures. Hussein Sayed and T.A. El-Sayed [21] carried out an investigation on the dynamics and stability of rotors supported on journal bearings; this analysis was based on the second order stiffness and damping coefficients present in the bearings. They used a flexible rotor model supported on two symmetrical journal bearings. Bearing parameters were identified using the direct solution of the Reynolds equation and using the time-dependent second-order perturbation method.

In addition, Michel Fliess and Hebertt Sira Ramírez [22] presented an approach known as algebraic identification, which allows for the development of identifiers addressing the online determination of unknown parameters supported by differential algebra along with operational calculus based on the mathematical model of the mechanical system.

Later, Mendoza Larios G. et al. [23], in a numerical approach, developed an estimator for the rotor dynamic coefficients by applying algebraic identification, in which the Finite Element Method was used to numerically obtain the response of the rotary system by using a multiple degrees-of-freedom (DOF) model. The proposed identifier requires the lateral displacements and the slope of the node located at the support to identify, as well as the slope of the adjacent node. The complexity of the experimental measurements of the nodal slopes complicates the implementation of the method. Recently, Baltazar Tadeo L. et al. [24] used the algebraic identification method to determine the magnitude and angular position of the unbalance in an asymmetric rotor-bearing system, taking as a basis for the algebraic identifier a mathematical model of an asymmetric rotor-bearing system of multiple degrees of freedom using active balancing disks. They tested the proposed identifier numerically and experimentally, demonstrating that it is possible to reduce the vibration amplitudes under resonance conditions of an asymmetric rotor by more than 95%.Therefore, Nango [25], Beltrán Carvajal et al. [26], Arias et al. [27], and Mendoza Larios G. et al. [28] proposed identifiers by using algebraic identification for the estimation of the parameters in rotor dynamic systems; both numerical and experimental results showed that the identification is quickly achieved and exhibits high robustness with regard to the parametric uncertainty. One of the main advantages of algebraic identification is that it provides identification relationships regardless of the initial conditions of the system and only requires the system response as the input data. The parameter identification is conducted online either in continuous or discrete time.

As can be seen, there are different investigations in the field of roto-dynamics where algebraic identification has been used to estimate some sought parameter; however, it has not been used to identify the dynamic coefficients of a pressurized bearing experimentally. Therefore, in the present work, a mathematical model was developed to identify the direct rotodynamic coefficients of a pressurized bearing at constant speed in a rotor-bearing system. The mathematical model was developed by applying the algebraic identification technique to a simplified two-degree-of-freedom model of a rotor-bearing system. Numerical and experimental simulations were carried out to test the functioning of the proposed algebraic identifier. It should be noted that this identifier of the direct rotodynamic coefficients only needs the lateral displacements of the node where the support to be identified is located. This is a great advantage since in the experimental part, the instrumentation is very easy to implement, and a minimum number of sensors is required. Another advantage of the proposed identifier is that it does not require the implementation of any external device to introduce some excitation force to the rotodynamic system since, as previously mentioned, the identification is made with the response of the system due to the unbalance, which is always present in all rotodynamic systems. The proposed algebraic identifier can be used in other types of bearings; in this case, it was used for a pressurized bearing, considering different operating speed and constant pressure. This means that it can be

used to identify the dynamic parameters of conventional bearings, where their dynamic coefficients are considered constant, or magnetic bearings, where their properties change depending on the current supplied to the support.

The rest of the document is organized as follows: in Section 2, two models are analyzed, the model of a rotor-bearing system with multiple degrees of freedom and the simplified model with two degrees of freedom, and a comparison is made between the responses of both models. In this same section, the algebraic identifier of the direct dynamic coefficients of a bearing is developed. Section 3 describes the simulation of the proposed identifier, numerically and experimentally. In this section, the identified coefficients are validated with the help of the models developed in the previous section. Section 4 shows a discussion section. Finally, Section 5 shows the conclusion of the research work presented.

2. Materials and Methods

2.1. Mathematical Model of the Rotor-Bearing System with Multiple DOFs

The mathematical model that represents the dynamic behavior of the multiple-DOF rotor-bearing system was derived according to the methodology proposed by Lalanne and Ferraris [29]. The shaft was modeled as a beam-type finite element with four DOFs per node: two lateral displacements (u_i, w_i) and two angular displacements (ψ_i, θ_i), see Figure 1.
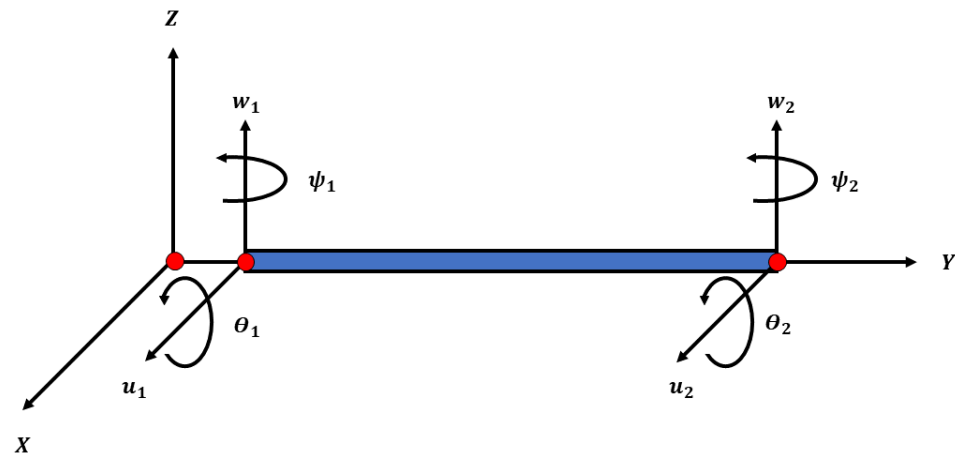

Figure 1. Beam-type finite element used for modeling the shaft.

The displacement and rotation vector per node is defined as follows:

$$\{\delta\} = \{u_1, w_1, \psi_1, \theta_1, u_2, w_2, \psi_2, \theta_2\}^T \tag{1}$$

In Equation (1), "*T*" denotes transpose. The displacements and rotations along the *X* and *Z* axes are defined as:

$$\begin{aligned}\{\delta_u\} &= \{u_1, \psi_1, u_2, \psi_2\}^T \\ \{\delta_w\} &= \{w_1, \theta_1, w_2, \theta_2\}^T\end{aligned} \tag{2}$$

According to Lalanne and Ferraris [29], the mathematical model of a rotor-bearing system dynamic behavior with multiple DOFs, which considers both unbalance as the exciting force and coasting up, can be written as:

$$[M]\{\ddot{\delta}\} + [C(\Omega)]\{\dot{\delta}\} + \left[K\left(\ddot{\phi}\right)\right]\{\delta\} = \Omega^2\{F_{u(1)}(\phi)\} + \ddot{\phi}\{F_{u(2)}(\phi)\} \tag{3}$$

where

$$\begin{aligned} F_{u(1)} &= m_u d(\sin(\phi + \alpha) + \cos(\phi + \alpha)) \\ F_{u(2)} &= m_u d(\sin(\phi + \alpha) - \cos(\phi + \alpha)) \end{aligned}$$

and where m_u, d and α are the mass, eccentricity, and angular position of the unbalance, respectively, and $\phi = \Omega t$. Additionally, $\{\delta\}$ is the vector containing the nodal displacements,

$[M]$ is the global mass matrix of the system, $[C(\Omega)]$ is the global damping matrix containing the gyroscopic effects as a function of the angular speed $\left(\dot{\phi}[C_2]\right)$, and $[C_1]$ contains the damping attributable to the supports. $\left[K\left(\ddot{\phi}\right)\right]$ is the global stiffness matrix, which is integrated by $[K_1], [K_2]$, which includes the stiffness of the bearing and the rotor, respectively, and by $\ddot{\phi}[K_3]$, which is the stiffness matrix as a function of the angular acceleration of the rotor. Finally, $\left\{F_{u(1)}(\phi)\right\}$ and $\left\{F_{u(2)}(\phi)\right\}$ denote the vectors of the centrifugal force components generated by the unbalance mass.

2.2. Mathematical Model of the 2-DOF Rotor-Bearing System

The mathematical model proposed by Lalanne and Ferraris [29] for a simple rotor dynamic system was considered in the present study. The rotor is supposed to be simply supported at both ends, as shown in Figure 2. In this figure, $R_0(XZY)$ is the inertial frame, and the rotor axis is along the Y axis, where Ω denotes the speed of rotation. The rotor-bearing system consists of a symmetric shaft of length L, a symmetric disk with an unbalance mass placed at $y = l_1$, and a journal bearing placed at $y = l_2$. The expressions for the displacements in the x and z directions are respectively:

$$
\begin{aligned}
u(y,t) &= f(y)q_1(t) = f(y)q_1 \\
w(y,t) &= f(y)q_2(t) = f(y)q_2
\end{aligned}
\tag{4}
$$

where q_1 and q_2 are generalized independent coordinates. As the angular displacements ψ and θ (Figure 1) are small, they are approximated by:

$$
\theta = \frac{\partial w}{\partial y} = \frac{df(y)}{dy}q_2 = g(y)q_2
\tag{5}
$$

$$
\psi = -\frac{\partial u}{\partial y} = \frac{df(y)}{dy}q_1 = -g(y)q_1
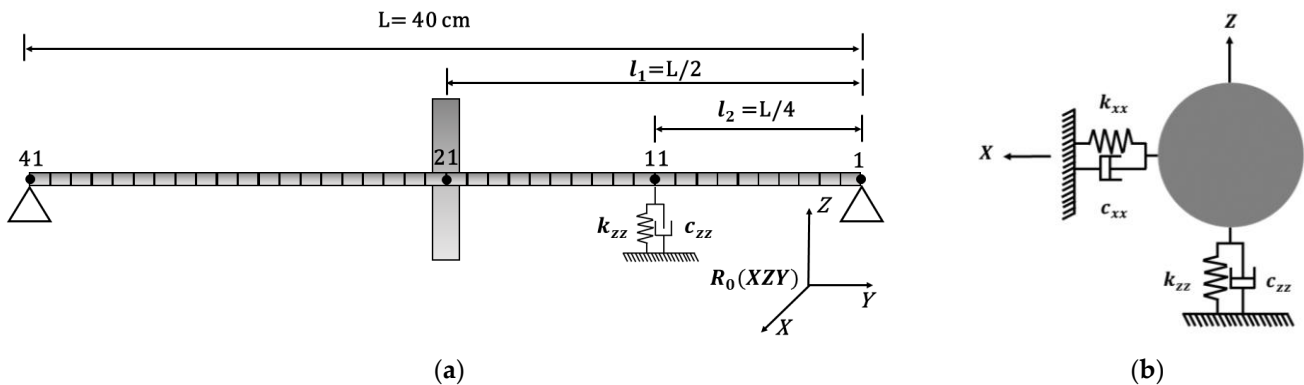\tag{6}
$$

Figure 2. The model of a bearing-rotor system. (**a**) Discretized rotor. (**b**) Node 11.

The second-order derivatives of u and w are necessary to express the strain energy; their expressions are:

$$
\frac{\partial^2 u}{\partial z^2} = \frac{d^2 f(y)}{dy^2}q_1 = h(y)\,q_1
\tag{7}
$$

$$
\frac{\partial^2 w}{\partial z^2} = \frac{d^2 f(y)}{dy^2}q_2 = h(y)q_2
\tag{8}
$$

The displacement chosen is the first modal shape of a beam with a constant cross-section in bending, simply supported at both ends, and it is given by:

$$f(y) = sin(\pi y/L) \tag{9}$$

In addition, the kinetic energy E_k, the strain energy U, and the virtual work δW of the external forces are calculated for the elements of the rotor-bearing system (Appendix A). The rotor equations come from the Lagrange's equations:

$$\frac{d}{dt}\left(\frac{\partial E_k}{\partial \dot{q}_i}\right) - \frac{\partial E_k}{\partial q_i} + \frac{\partial U}{\partial q_i} = Fq_i \tag{10}$$

where $N(1 \leq i \leq N)$ is the number of degrees of freedom, q_i are generalized independent coordinates, Fq_i are generalized forces, and $\cdot$ denotes differentiation with respect to time t.

As stated by Lalanne and Ferraris [29], the mathematical model corresponding to the rotor-bearing system, shown in Figure 2, is given by:

$$\begin{aligned}
m\ddot{q}_1 - a\Omega\dot{q}_2 + c_{xx}f^2(l_2)\dot{q}_1 + k_r q_1 + k_{xx}f^2(l_2)q_1 \\
= m_u df(l_1)(\Omega^2 sin(\Omega t + \alpha) - \ddot{\phi}cos(\Omega t + \alpha)) \\
m\ddot{q}_2 + a\Omega\dot{q}_1 + c_{zz}f^2(l_2)\dot{q}_2 + k_r q_2 + k_{zz}f^2(l_2)q_2 - a\ddot{\phi}q_2 \\
= m_u df(l_1)\left(\Omega^2 cos(\Omega t + \alpha) + \ddot{\phi}sin(\Omega t + \alpha)\right)
\end{aligned} \tag{11}$$

In a matrix form,

$$[M]\{\ddot{q}\} + \left([C_1]f^2(l_2) + [C_2(\Omega)]\right)\{\dot{q}\} + \left([K_1]f^2(l_2) + [K_2] + \left[K_3\left(\ddot{\phi}\right)\right]\right)\{q\} = \{F\} \tag{12}$$

with

$$[M] = \begin{bmatrix} m & 0 \\ 0 & m \end{bmatrix}; [C_1] = \begin{bmatrix} c_{xx} & 0 \\ 0 & c_{zz} \end{bmatrix}; f_1 = m_u df(l_1)(\Omega^2 sin(\Omega t + \alpha) - \ddot{\phi}cos(\Omega t + \alpha))$$

$$[C_2] = \begin{bmatrix} 0 & -a \\ a & 0 \end{bmatrix}; [K_1] = \begin{bmatrix} k_{xx} & 0 \\ 0 & k_{zz} \end{bmatrix}; f_2 = m_u df(l_1)\left(\Omega^2 cos(\Omega t + \alpha) + \ddot{\phi}sin(\Omega t + \alpha)\right)$$

$$[K_2] = \begin{bmatrix} k_r & 0 \\ 0 & k_r \end{bmatrix}; [K_3] = \begin{bmatrix} 0 & -a\ddot{\phi} \\ 0 & 0 \end{bmatrix}; a = I_{Dy}g^2(l_1) + 2\rho I \int_0^L g^2(y)dy$$

$$\{q\} = \begin{Bmatrix} q_1 \\ q_2 \end{Bmatrix}; \{F\} = \begin{Bmatrix} f_1 \\ f_2 \end{Bmatrix}$$

The parameters m and a are defined in Equation (A5). Other parameters are defined as follows:
c_{ij} = bearing damping [N·s·m^{-1}]
k_{ij} = bearing stiffness [N·m^{-1}]
$m_u d$ = unbalance [kg·m]
Ω = angular frequency of the rotor [s^{-1}]
α = mass unbalance angular position [degrees]
k_r = stiffness of the rotor [N·m^{-1}]

For the present analysis, the coefficients k_{xx}, k_{zz}, and c_{xx}, c_{zz}, corresponding to the matrices $[K_1]$ and $[C_1]$, vary as a function of both the rotor angular frequency Ω and the bearing pressure. The C_2 matrix multiplied by Ω gives the gyroscopic effect.

2.3. Comparison between the Multiple-DOF and the Simplified 2-DOF Models

In this section, a comparison between the solution obtained by using the multiple-DOF model given in Equation (3) and that obtained by using the simplified two-DOF model given in Equation (12) is presented. The mechanical and geometrical properties of the simulated rotor are presented in Table 1. For practical purposes in the numerical simulation, it was considered that the rotor dynamic coefficients of the support in node 11 (see Figure 2) are constant, as presented in Table 2. In addition, lineal coasting up $\Omega = \ddot{\phi}t + \Omega_0$, where $\ddot{\phi} = 25$ rad/s^2 and $\Omega_0 = 0$ was considered. The vibration

response for node 21 (see Figure 2) obtained by using the two-DOF model was compared to the vibration response obtained by using the multiple-DOF model.

Table 1. Mechanical and geometrical properties of the rotor.

Mechanical Properties	Geometrical Properties of the Shaft	Geometrical Properties of the Disk	
$E = 2 \times 10^{11} \text{ N/m}^2$	Radius $r_s = 0.01 \text{ m}$	e_D	0.03 m
$\rho = 7800 \text{ kg/m}^3$	$L = 0.40 \text{ m}; L_e = 0.01 \text{ m}$	r_{iD}	0.01 m
$v = 0.30$	$l_1 = 0.20 \text{ m}; L_2 = 0.10 \text{ m}$	r_{eD}	0.15 m

Table 2. Dynamic coefficients of the bearing at node 11.

Stiffness (N/m)	Damping (Ns/m)
$k_{xx} = 2 \times 10^5$	$c_{xx} = 3 \times 10^2$
$k_{xz} = k_{zx} = 0$	$c_{xz} = c_{zx} = 0$
$k_{zz} = 5 \times 10^5$	$c_{zz} = 7.5 \times 10^2$

The vibration response of the rotor obtained by using the multiple-DOF and the simplified two-DOF models are depicted in Figure 3. It is possible to observe that both the vibration responses depicted in Figure 3 are quite similar during the operation interval of the rotor, and the higher differences are achieved close to resonance (2500 < rpm < 3000). By comparing these vibration responses, it is possible to conclude that the 2-DOF simplified model can be used for identifying the rotor dynamic coefficients in order to decrease computational costs and reduce the number of sensors required for acquiring the vibration signal since the multiple-DOF model needs to experimentally acquire the signal of two displacements as well as two rotations per node, which is complicated.
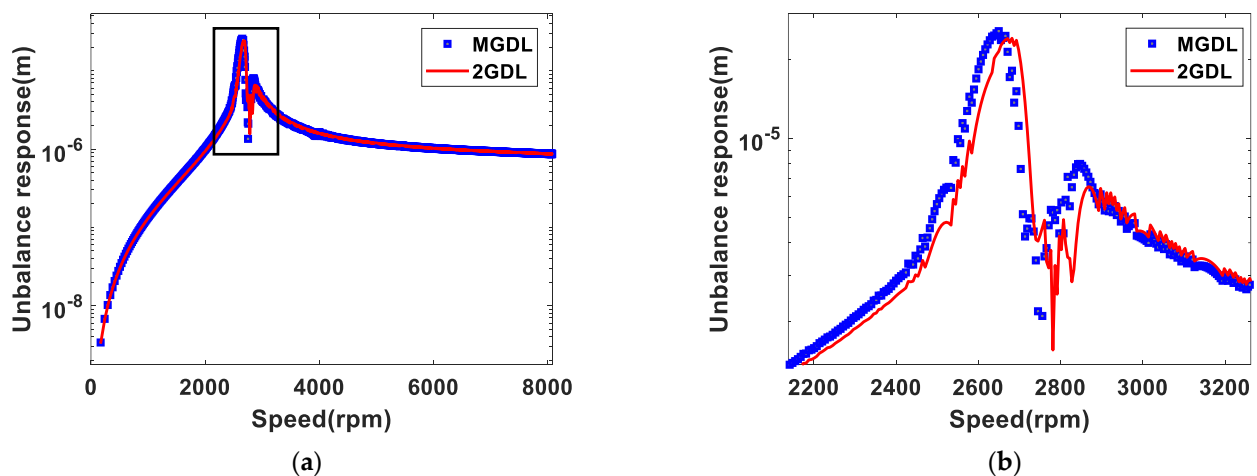
Figure 3. Comparison between the vibration response obtained by the multiple-DOF model and by the 2-DOF simplified model at node 21. $\ddot{\phi} = 25 \text{ rad/s}^2$. (**a**) Vibration response from 0 to 8000 rpm. (**b**) Vibration response in the resonance zone.

2.4. Mathematical Model for the Online Algebraic Identification of the Direct Dynamic Coefficients of a Bearing in a Rotor-Bearing System at a Constant Speed

It is well known that the dynamic behavior of rotating machines is strongly influenced by the bearing properties since the stiffness of the rotor-bearing system is the result of the bearing stiffness and the shaft stiffness addition. Likewise, the damping of the system is mainly the result of the bearing damping properties.

Algebraic identification (AI) is a method based on both differential algebra and operational calculus aimed at the development of estimators, which allows for the determination of unknown parameters of a system from its mathematical model. The online identifier was developed from the

mathematical model that describes the dynamic behavior of the rotor given in Equation (12). If the angular speed Ω is constant, Equation (12) can be written as:

$$
\begin{aligned}
m\ddot{q}_1 - a\Omega\dot{q}_2 + c_{xx}f^2(l_2)\dot{q}_1 + k_r q_1 + k_{xx}f^2(l_2)q_1 = m_u f(l_1)d\Omega^2\sin\Omega t \\
m\ddot{q}_2 + a\Omega\dot{q}_1 + c_{zz}f^2(l_2)\dot{q}_2 + k_r q_2 + k_{zz}f^2(l_2)q_2 = m_u f(l_1)d\Omega^2\cos\Omega t
\end{aligned}
\tag{13}
$$

In a matrix form:

$$
[M]\{\ddot{q}\} + \left([C_1]f^2(l_2) + [C_2(\Omega)]\right)\{\dot{q}\} + \left([K_1]f^2(l_2) + [K_2]\right)\{q\} = \{F\}
\tag{14}
$$

with

$$
\{F\} = \begin{Bmatrix} f_1 \\ f_2 \end{Bmatrix} = \begin{Bmatrix} m_u f(l_1)d\Omega^2\sin\Omega t \\ m_u f(l_1)d\Omega^2\cos\Omega t \end{Bmatrix}
$$

$$
\{\delta\} = \begin{Bmatrix} u_i \\ w_i \end{Bmatrix}
$$

According to Fliess and Sira-Ramírez [20], Equation (14) is multiplied by t^2 and the integrated twist in time t, which yields the base mathematical model presented in Equation (15).

$$
\begin{aligned}
f^2(l_2)[K_1]\textstyle\int^{(2)} t^2\{\delta\} + f^2(l_2)[C_1]\left(\int t^2\{\delta\} - 2\int^{(2)} t\{\delta\}\right) \\
= -[M]t^2\delta + 4[M]\int t\delta - \Omega[C_2]\int t^2\delta - 2[M]\int^{(2)}\delta \\
+ 2\Omega[C_2]\int^{(2)} t\delta - [K_2]\int^{(2)} t^2\{\delta\} + \int^{(2)} t^2\{F\}
\end{aligned}
\tag{15}
$$

By analyzing Equation (15), it can be observed that there are 4 unknown values (k_{xx}, k_{zz}, c_{xx}, c_{zz}) in 2 equations; therefore, Equation (15) is integrated once more in order to form the system of 4 equations with 4 unknown values as presented in Equation (16).

$$
\begin{aligned}
f^2(l_2)[K_2]\textstyle\int^{(3)} t^2\{\delta\} + f^2(l_2)[C_1]\left(\int^{(2)} t^2\{\delta\} - 2\int^{(3)} t\{\delta\}\right) \\
= -[M]\int t^2\delta + 4[M]\int^{(2)} t\delta - \Omega[C_2]\int^{(2)} t^2\delta - 2[M]\int^{(3)}\delta \\
+ 2\Omega[C_2]\int^{(3)} t\delta - [K_2]\int^{(3)} t^2\{\delta\} + \int^{(3)} t^2\{F\}
\end{aligned}
\tag{16}
$$

where $\int^{(N)} \varphi(\sigma_N)$ are iterated integrals of the form $\int_0^t \int_0^{\sigma_1}\cdots\int_0^{(\sigma_{N-1})} \varphi(\sigma_N)d\sigma_N\cdots d\sigma_1$, with $\int \varphi(t) = \int_0^t \varphi(\sigma)d\sigma$, and N is a positive integer.

From Equations (15) and (16), an equation system is obtained in the form:

$$
\begin{aligned}
A(t)\Theta_1 = B_1(t) \\
P(t)\Theta_2 = B_2(t)
\end{aligned}
\tag{17}
$$

$$
\begin{aligned}
A(t) = \begin{bmatrix} a_{11}(t) & a_{12}(t) \\ a_{21}(t) & a_{22}(t) \end{bmatrix} \quad\quad B_1(t) = \begin{Bmatrix} b_1(t) \\ b_2(t) \end{Bmatrix} \quad\quad \Theta_1 = \begin{Bmatrix} k_{xx} \\ c_{xx} \end{Bmatrix} \\
P(t) = \begin{bmatrix} p_{11}(t) & p_{12}(t) \\ p_{21}(t) & p_{22}(t) \end{bmatrix} \quad\quad B_2(t) = \begin{Bmatrix} b_3(t) \\ b_4(t) \end{Bmatrix} \quad\quad \Theta_2 = \begin{Bmatrix} k_{zz} \\ c_{zz} \end{Bmatrix}
\end{aligned}
\tag{18}
$$

$$
\begin{aligned}
a_{11}(t) = \textstyle\int^{(2)} t^2 u_i dt; \quad\quad\quad a_{12}(t) = \int t^2 u_i dt - 2\int^{(2)} t u_i dt \\
a_{21}(t) = \textstyle\int^{(3)} t^2 u_i dt; \quad\quad\quad a_{22}(t) = \int^{(2)} t^2 u_i dt - 2\int^{(3)} t u_i dt
\end{aligned}
\tag{19}
$$

where

$$
\begin{aligned}
p_{11}(t) = \textstyle\int^{(2)} t^2 w_i dt; \quad\quad\quad p_{12}(t) = \int t^2 w_i dt - 2\int^{(2)} t w_i dt \\
p_{21}(t) = \textstyle\int^{(3)} t^2 w_i dt; \quad\quad\quad p_{22}(t) = \int^{(2)} t^2 w_i dt - 2\int^{(3)} t w_i dt
\end{aligned}
\tag{20}
$$

$$
\begin{aligned}
b_1 = -[M]t^2 u_i + 4[M]\textstyle\int t u_i - \Omega[C_2]\int t^2 u_i - 2[M]\int^{(2)} u_i \\
+ 2\Omega[C_2]\int^{(2)} t u_i - [K_2]\int^{(2)} t^2 u_i + \int^{(2)} t^2\{F\} \\
b_2 = -[M]\int t^2 u_i + 4[M]\int^{(2)} t u_i - \Omega[C_2]\int^{(2)} t^2 u_i - 2[M]\int^{(3)} u_i \\
+ 2\Omega[C_2]\int^{(3)} t u_i - [K_2]\int^{(3)} t^2 u_i + \int^{(3)} t^2\{F\}
\end{aligned}
\tag{21}
$$

$$
\begin{aligned}
b_3 = {} & -[M]t^2 w_i + 4[M]\int tw_i - \Omega[C_2]\int t^2 w_i - 2[M]\int^{(2)} w_i \\
& +2\Omega[C_2]\int^{(2)} tw_i - [K_2]\int^{(2)} t^2 w_i + \int^{(2)} t^2\{F\} \\
b_4 = {} & -[M]\int t^2 w_i + 4[M]\int^{(2)} tw_i - \Omega[C_2]\int^{(2)} t^2 w_i - 2[M]\int^{(3)} w_i \\
& +2\Omega[C_2]\int^{(3)} tw_i - [K_2]\int^{(3)} t^2 w_i + \int^{(3)} t^2\{F\}
\end{aligned}
\tag{22}
$$

where $\Theta_1 = \{k_{xx}, c_{xx}\}^T$ and $\Theta_2 = \{k_{zz}, c_{zz}\}^T$ denote the rotor dynamic parameters vector to identify, and with $A(t)$ and $P(t)$ as 2×2 matrices and $B_1(t)$ and $B_2(t)$ as 2×1 vectors, which are obtained from Equations (15) and (16). It can be noted that $A(t)$, $P(t)$, $B_1(t)$ and $B_2(t)$ are functions of the rotor response $\{\delta\}$.

From Equation (17), it can be noted that vectors Θ_1 and Θ_2 are algebraically identifiable if, and only if, the trajectory of the dynamic system complies with the condition established by Fliess and Sira-Ramírez [22]. This condition means that the trajectories of the dynamic behavior of the system satisfy the conditions $det[A(t) \neq 0]$ and $det[P(t) \neq 0]$. Generally, this condition is accomplished at least during a small interval $(t_0, t_0 + \epsilon)$, where ϵ is small and positive.

The online identifier model is obtained by solving Equation (17) for Θ_1 and Θ_2, which allows for the determination of the rotor dynamic coefficients of the two-degrees-of-freedom rotor-bearing system.

$$
\left.
\begin{aligned}
\Theta_1 &= A^{-1}(t)B_1(t) \\
\Theta_2 &= P^{-1}(t)B_2(t)
\end{aligned}
\right\} \forall t \in (t_0, t_0 + \in]
\tag{23}
$$

As can be observed in Equation (23), algebraic identification of the rotor dynamic coefficients is independent of the boundary conditions and depends only on the system displacement vectors in directions x and z for each time t, as well as the rotor angular frequency Ω.

3. Results

In this section, the operation of the proposed algebraic identifier of the rotodynamic coefficients is shown numerically and experimentally. The identification process is carried out at constant speed and at different operating speeds of the rotor. The identified rotodynamic coefficients are shown in Table 3 (numerical results) and Table 4 (experimental results). It is important to point out that the proposed identifier estimates only the direct rotodynamic coefficients (k_{xx}, k_{zz}, c_{xx}, c_{zz}); this is because a simplified mathematical model is used to develop the algebraic identifier, since it is the purpose of this research to identify the rotodynamic coefficients in a fast, simple way and with acceptable results.

Table 3. Identified dynamic coefficients and their errors.

Speed (rpm)	k_{xx}	$\varepsilon(\%)$	k_{zz}	$\varepsilon(\%)$	c_{xx}	$\varepsilon(\%)$	c_{zz}	$\varepsilon(\%)$
1200	2.30×10^5	15.19	5.67×10^5	13.37	3.34×10^2	11.36	8.38×10^2	11.79
2400	1.57×10^5	21.52	4.54×10^5	9.21	2.96×10^2	1.38	7.38×10^2	1.73
2800	1.30×10^5	34.95	4.01×10^5	19.72	3.01×10^2	1.97	6.98×10^2	7.03

Stiffness (N/m) − damping (Ns/m).

Table 4. Mechanical and geometrical properties of the experimental rotor.

Mechanical Properties	**Geometrical Properties of the Shaft**		**Geometrical Properties of the Disk**	
$E = 2 \times 10^{11}$ N/m^2	*Radius* $r_s = 0.005$ m		e_D	0.025 m
$\rho = 7800$ kg/m^3	$L = 0.40$ m; $L_e = 0.01$ m		r_{iD}	0.005 m
$v = 0.30$	$l_1 = 0.20$ m; $L_2 = 0.10$ m		r_{eD}	0.0375 m

3.1. Numerical Results

The vibration response of the rotor-bearing system used in the algebraic identification (AI) of the rotodynamic coefficients (node 11) was obtained from Equation (3) using the Newmark direct integration method under a constant velocity scheme, with time increments of 1×10^{-4}, which is equivalent to 1×10^4 samples per second. The rotor used in this simulation is the same as that used in Section 2.1 (see Figure 2), and the rotor dynamic coefficients of the bearing at node 11 are those presented in Table 2.

The rotor vibration response acquired from axis *X* and *Z*, specifically, from node 11 (see Figure 2a), is used as input data in the proposed identifying model presented in Equation (17). The algebraic identifier requires the vibration response of the node where the support to be identified is located; in this case, it is node 11. The behavior of the identifier as a function of time is depicted in Figure 4; the value of the identified rotor dynamic coefficient is represented by the red line, while the actual value is represented by the blue line. It is possible to observe in Figure 4 that the identifier (red line) converges to a constant value in less than 0.2 s, which demonstrates that the identifier achieves a real value in less than 0.2 s. The difference between the real parameter and the identified parameter of Figures 4–6 is because, for the development of the proposed identifier in Equation (17), a simplified model of two degrees of freedom from Equation (12) is taken as a basis. For the identification process, the vibration response obtained numerically by solving the equation of motion of the rotor-bearing system with multiple degrees of freedom in Equation (3) is used. Figure 3 shows a comparison between the responses obtained using a simplified model and using the multiple-degrees-of-freedom model. It is observed that their behavior is similar, but there are differences in their amplitudes, which are more noticeable in the resonance zone. For this reason, it is expected that in the resonance zone, there will be greater differences between the identified parameters and the real ones.
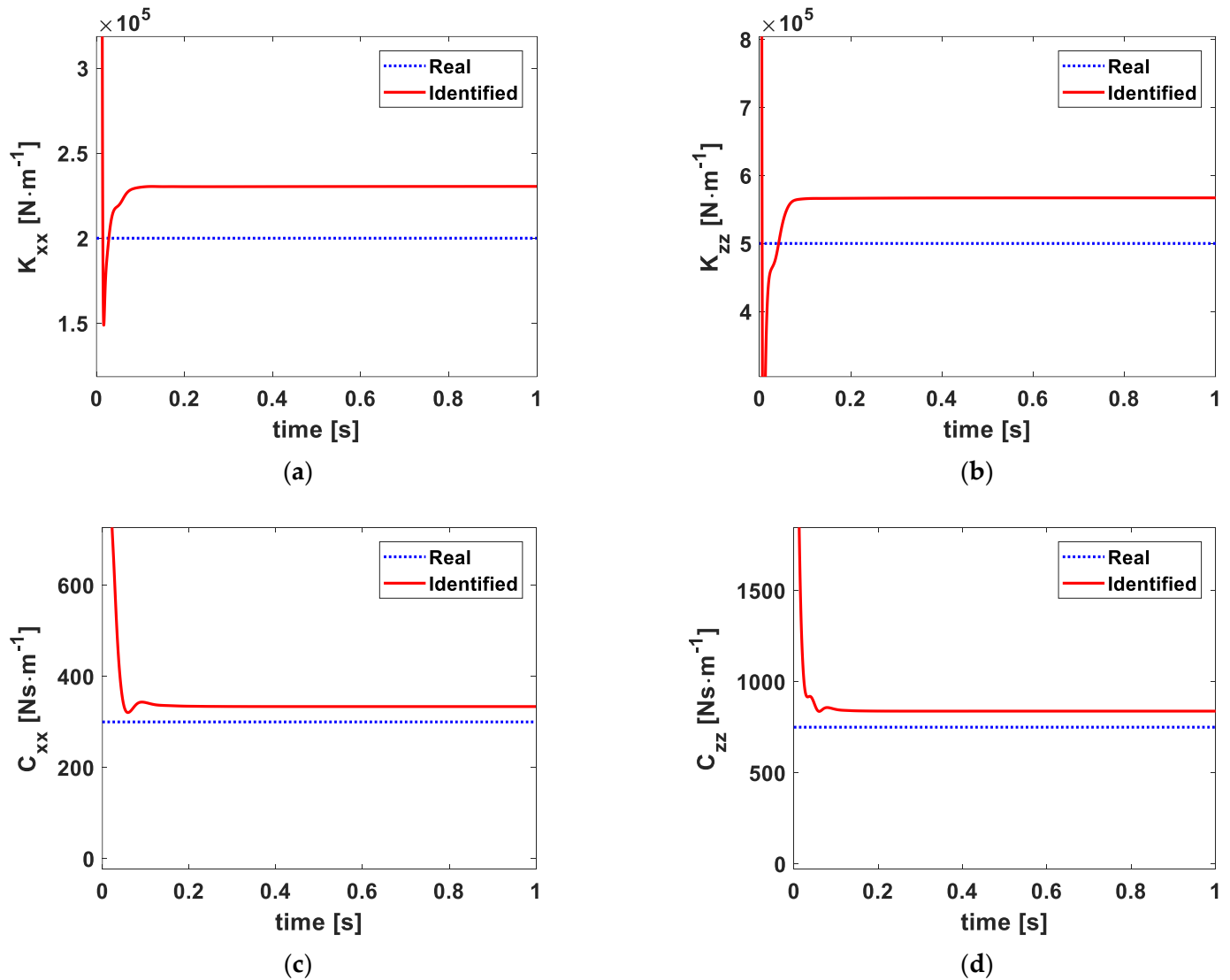

Figure 4. Identified rotor dynamic coefficients at 1200 rpm. (**a**) k_{xx}, (**b**) k_{zz}, (**c**) c_{xx}, (**d**) c_{zz}.
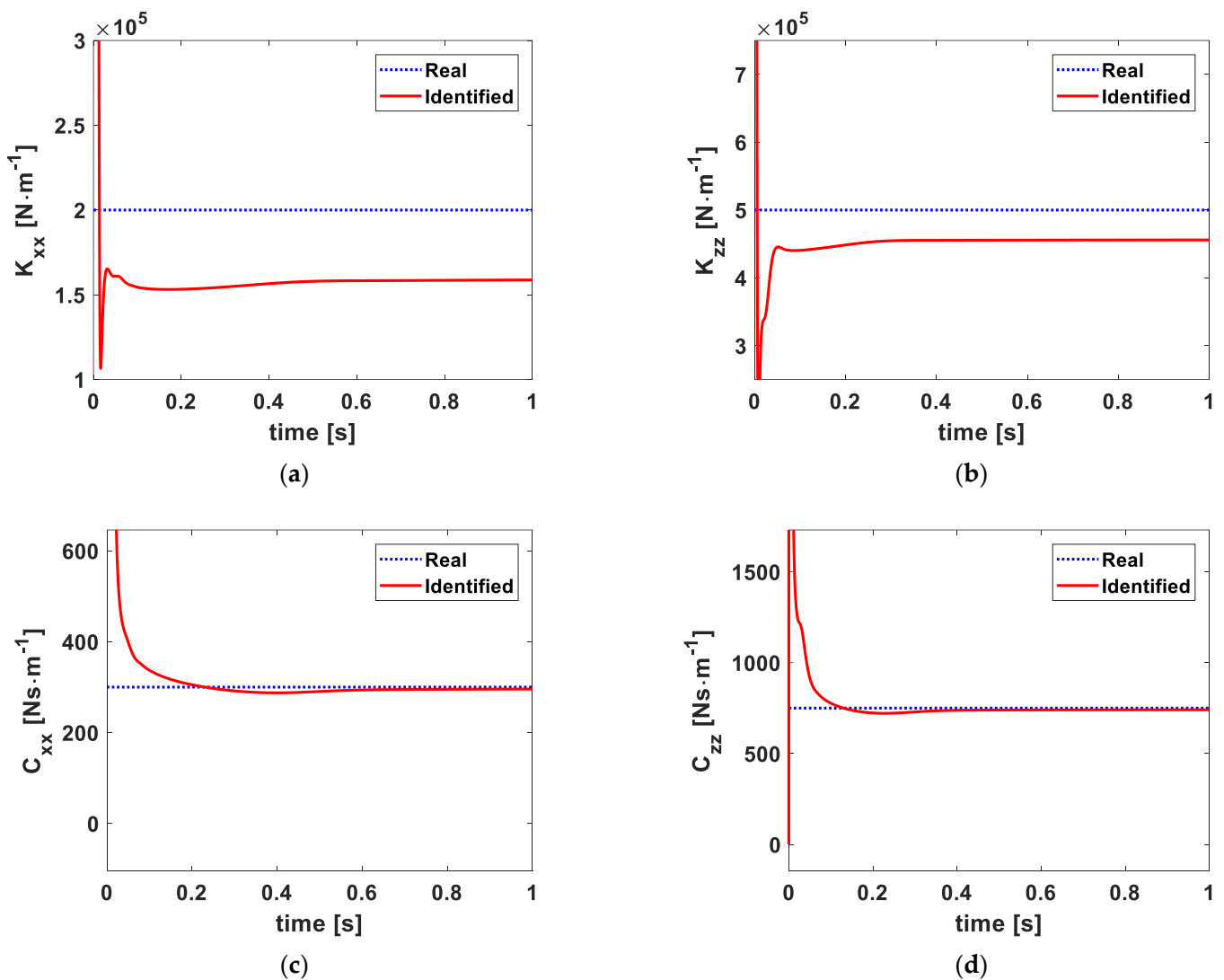
Figure 5. Identified rotor dynamic coefficients at 2400 rpm. (**a**) k_{xx}, (**b**) k_{zz}, (**c**) c_{xx}, (**d**) c_{zz}.

The rotor vibration response was obtained using the rotor dynamic coefficients identified by AI in the 2-DOF model presented in Equation (11) at 1200 rpm, 2400 rpm, and 2800 rpm. The comparison between the vibration response obtained numerically using the rotor dynamic-identified coefficients and that obtained numerically using the rotor dynamic coefficients presented in Table 2 is depicted in Figures 7–9. It is possible to observe in these figures that the behavior of both vibration responses is quite similar, which proves that the identified value of the dynamic coefficients reproduce the dynamic behavior of the rotor, showing that the proposed identifier is effective.

It is well known that in a pressurized bearing, the value of the rotor dynamic coefficients is a function of both the pressure and the angular speed; however, as the aim was to assess the performance of the proposed identifier, the identification of the rotor dynamic coefficients at 2400 and 3000 rpm was conducted by taking into account that they are constant and that their values are those presented in Table 2.

The identified rotor dynamic coefficients of stiffness and damping and their error at three rotor speeds are presented in Table 3, where it is possible to note that the highest error in the stiffness coefficients is achieved when the identification is conducted at 2800 rpm; this is due to fact that the highest difference between the vibration response obtained by using the 2-DOF simplified model and that obtained by using the multiple-DOF model is exhibited close to resonance, as depicted in Figure 3.
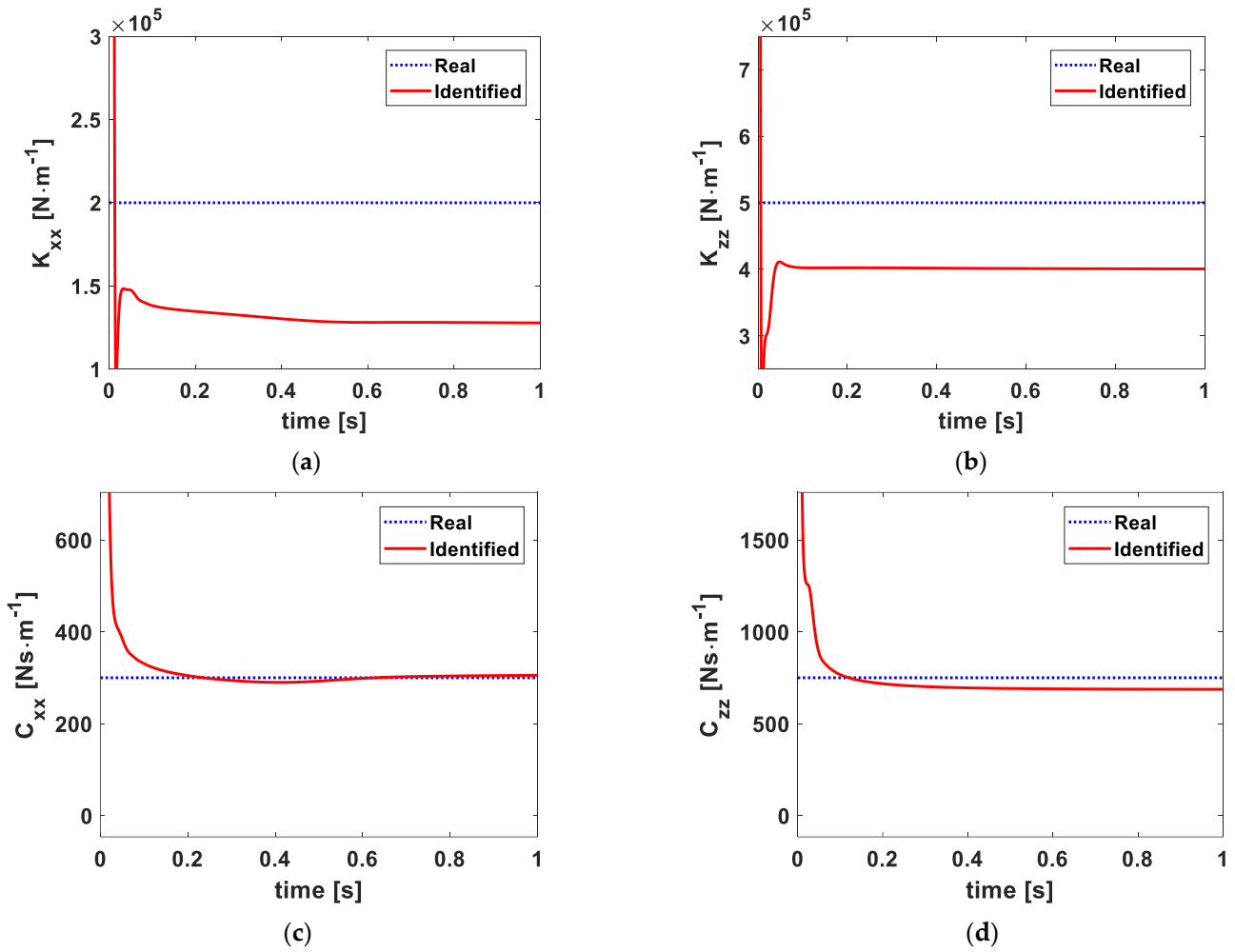
Figure 6. Identified rotor dynamic coefficients at 2800 rpm. (**a**) k_{xx}, (**b**) k_{zz}, (**c**) c_{xx}, (**d**) c_{zz}.
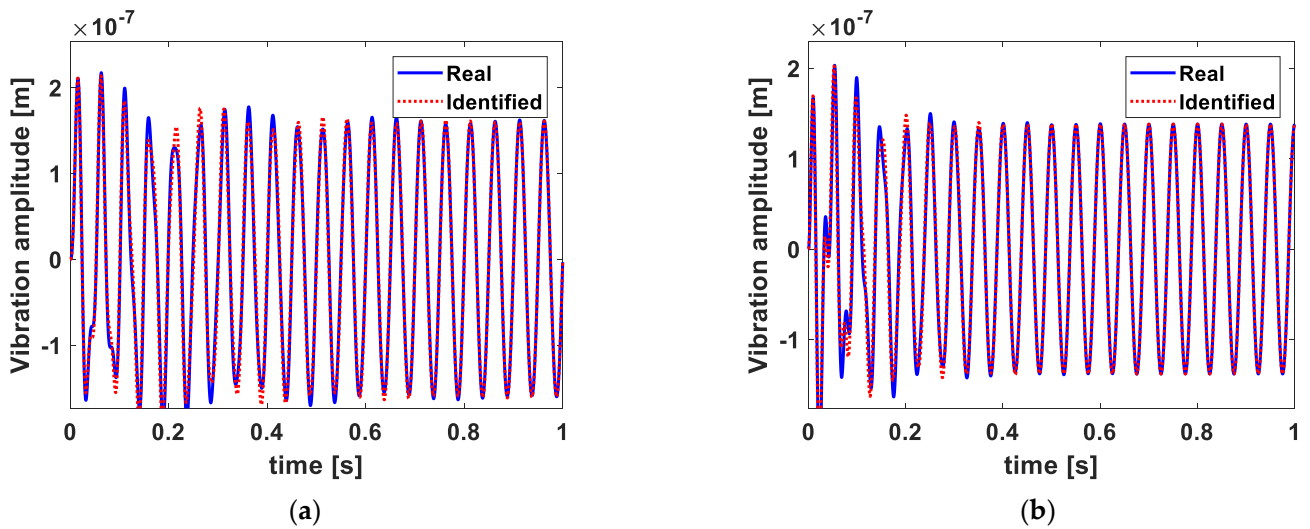

Figure 7. Comparison between the original vibration response and the vibration response obtained numerically using the identified rotor dynamics coefficients at 1200 rpm. (**a**) *X* direction and (**b**) *Z* direction.

Figure 8. Comparison between the original vibration response and the vibration response obtained numerically using the identified rotor dynamics coefficients at 2400 rpm. (**a**) *X* direction and (**b**) *Z* direction.
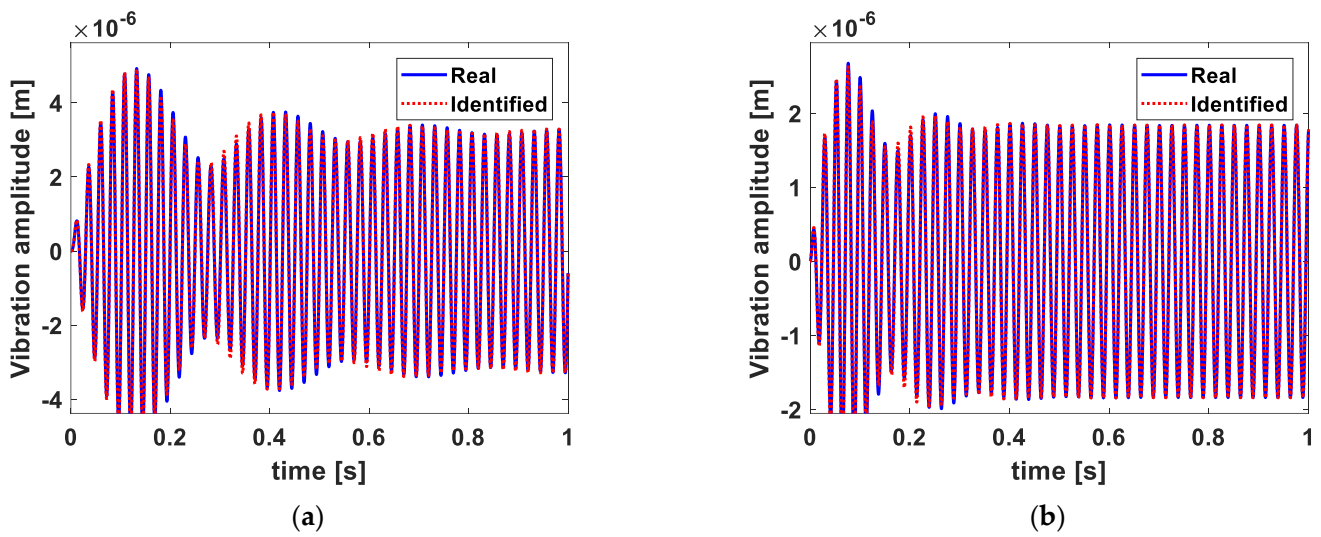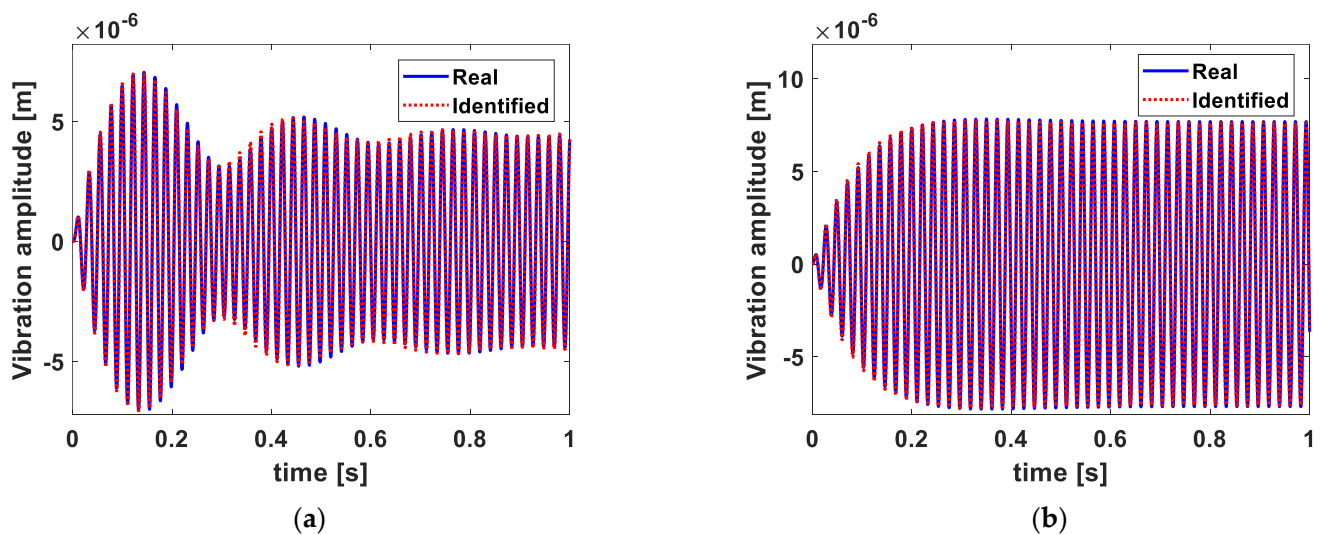

Figure 9. Comparison between the original vibration response and the vibration response obtained numerically using the identified rotor dynamics coefficients at 2800 rpm. (**a**) *X* direction and (**b**) *Z* direction.

3.2. Experimental Results

The behavior analysis of the proposed algebraic identifier as a function of time is presented in this section; the identifier was fed with the vibration response data experimentally acquired from the rotor at node 11 (see Figure 10). The discretization of the experimental rotor used is the same as that shown in Section 2.1 (see Figure 2). There are changes in the geometry of the disk and the shaft (see Table 4). The experimental rotor is supported at its ends (nodes 1 and 41) by a pair of identical bearings, which consists of a shaft of 40 cm in effective length discretized into 40 elements of 1 cm (41 nodes), an inertial disk at the middle (node 21), and a Bently Nevada pressurized bearing with a ratio $L_j/D = 1$ at node 11. In this pressurized bearing, its direct rotodynamic coefficients will be identified. This type of bearing has hydrostatic and hydrodynamic characteristics. A 10 psi constant pressure at the input of the bearing was considered in the analysis. The working fluid is Chevron GST 32 oil.

All the geometric and mechanical properties of the rotodynamic system within reach are considered to elaborate the numerical model of the experimental rotor (see Table 4). It is necessary to verify that it is faithful enough to ensure that the results are reliable. In the numerical model, it is considered that the supports at the ends of nodes 1 and 41 have a very high rigidity. To match this condition in the experimental part, two adjoining supports are placed at nodes 1 and 41 (see

Figure 10); this has the aim of avoiding slight angular movements and increasing the rigidity at the ends [30]. It is worth mentioning that the damping of the supports located at the ends (node 1 and 41) was neglected and the stiffness values used were 2×10^5 N/m. Numerically, with these properties of the end supports (node 1 and 41), the coefficients of Table 2 for the bearing located in node 11, and the geometric and mechanical properties of Table 1, a comparison was made between both the model of multiple degrees of freedom, which is what we have in the experimental part, and the model of two degrees of freedom, with which the algebraic identifier was developed. From this comparison, both answers are quite close and acceptable (see Figure 3), so there is a reliable model to work with. The vibration response (displacement) along the horizontal and vertical directions was acquired at node 11 by using Bently Nevada vibration sensors, Eddy Current type, with a sensitivity of 8 mV/μm and a data acquisition card National Instrument brand NI USB-6251, 16 Bits, 1.25 MS/s. The experimentally acquired vibration response, as well as the known rotor parameters, were used as input data in the proposed identifier model to identify the rotor dynamic parameter (Equation (20)).
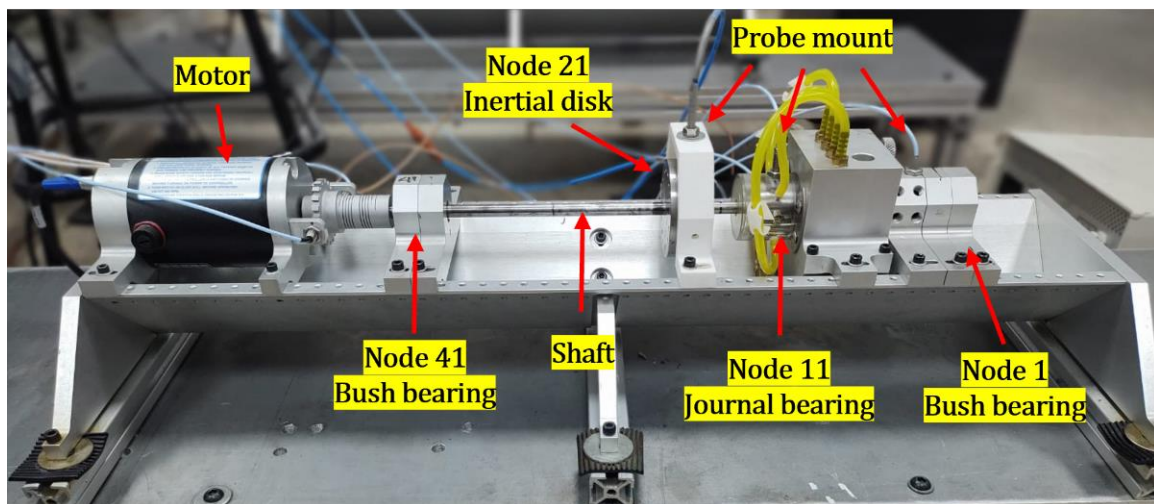

Figure 10. The experimental test rig.

The geometry and main characteristics of the pressurized bearing used for the experimental tests are found in Figure 11 and in Table 5.
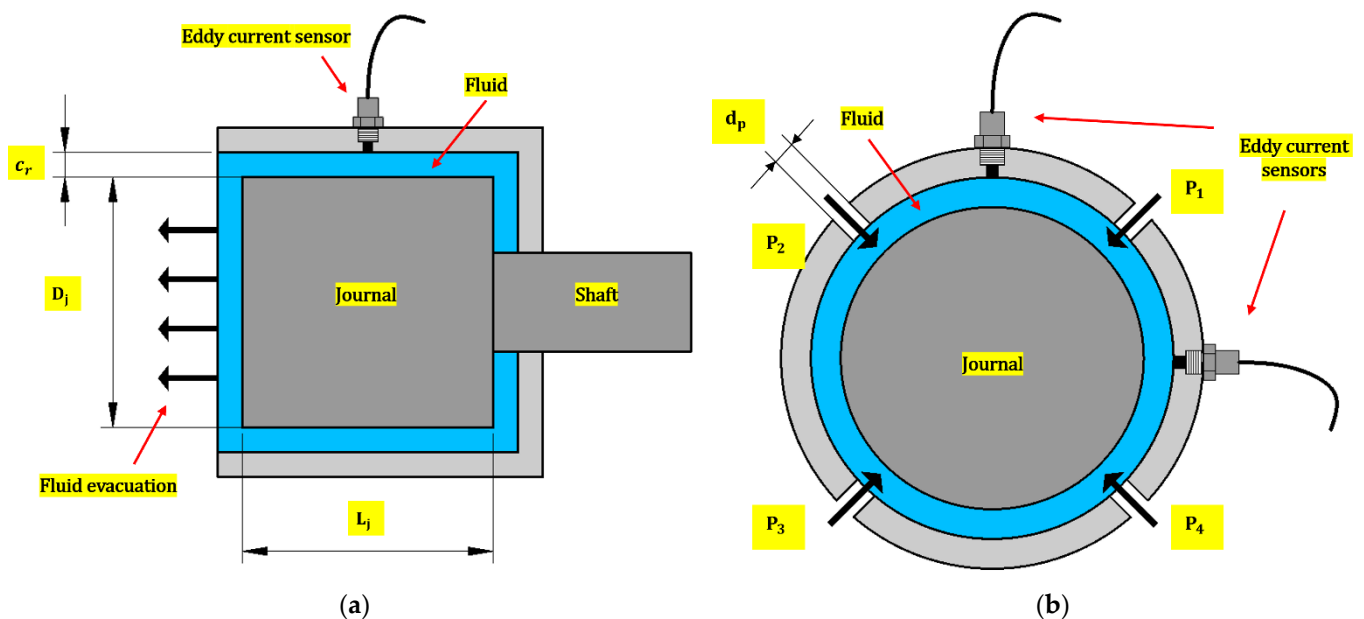

Figure 11. Schematic diagram of the journal bearing. Top view (**a**) and front view (**b**).

Table 5. Details of journal bearing for the experimental test.

Property	Assumed Value
Diameter D_j	25.4 mm
Length L_j	25.4 mm
Length-to-diameter ratio $\frac{L_j}{D_j}$	1
Radial clearance c_r	0.16 mm
Diameter (d_p) of the fluid injection ports (P_1, P_2, P_3, P_4)	2 mm

The rotor dynamic parameter identification for a rotor speed of 2400 rpm is depicted in Figure 12. It can be observed in Figure 12 that the identification obtained using the experimental vibration response describes a similar behavior to that obtained by the numerical simulation. It can be also noted that the identifier converges to a constant value in less than 0.1 s.
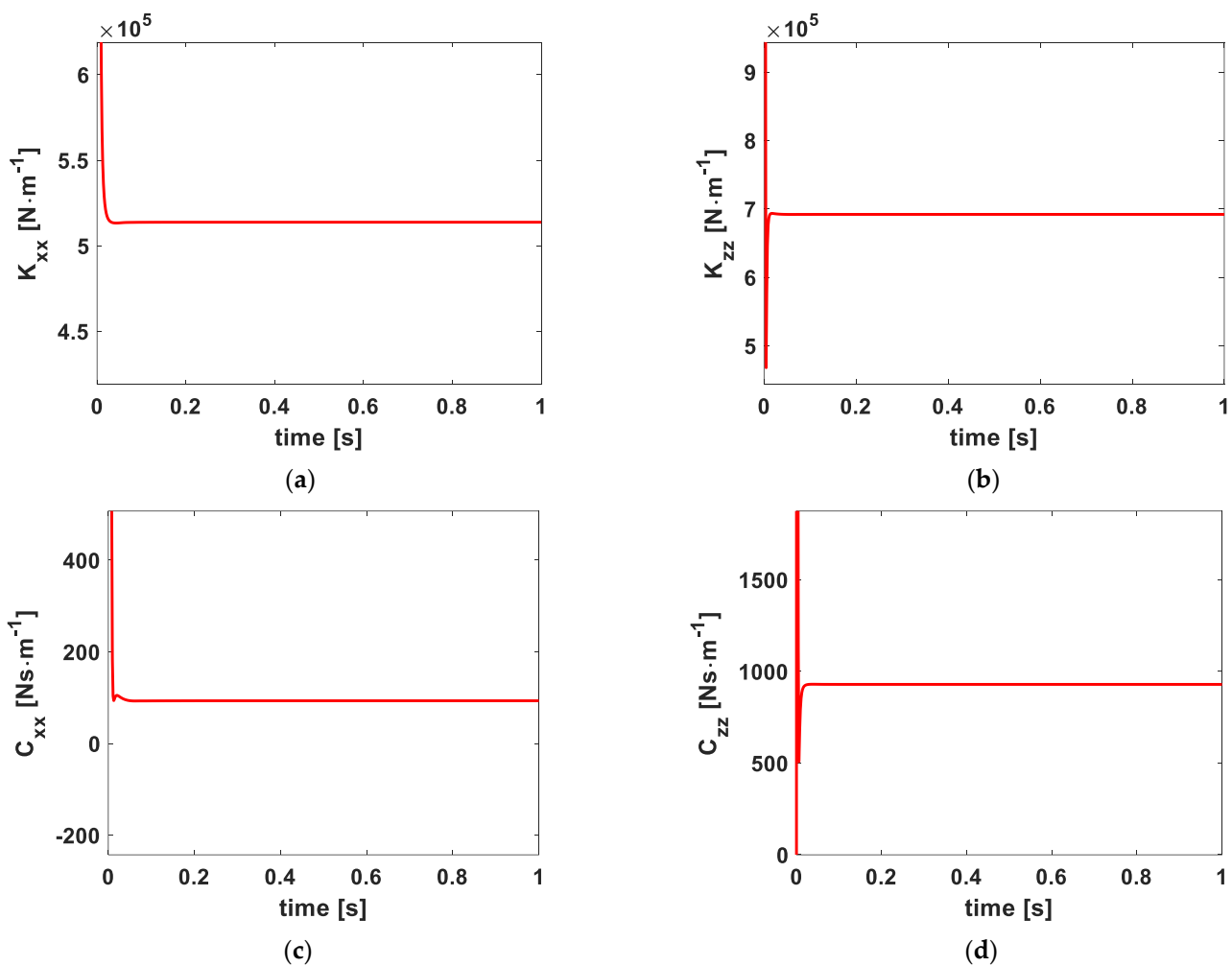
Figure 12. Direct identified rotor dynamic coefficients of stiffness and damping at 2400 rpm. (**a**) k_{xx}, (**b**) k_{zz}, (**c**) c_{xx}, (**d**) c_{zz}.

To validate the identified rotor dynamic parameters depicted in Figure 12, the identified values by AI were taken as input data, and a vibration response was numerically generated using the dynamic behavior model of a 2-DOF rotor presented in Equation (11), which was then compared to that experimentally acquired at 2400 rpm. The comparison of the vibration responses is depicted in Figure 13, where it can be observed that the identified rotor dynamic parameters properly reproduce the experimental vibration response of the rotor with a small error.
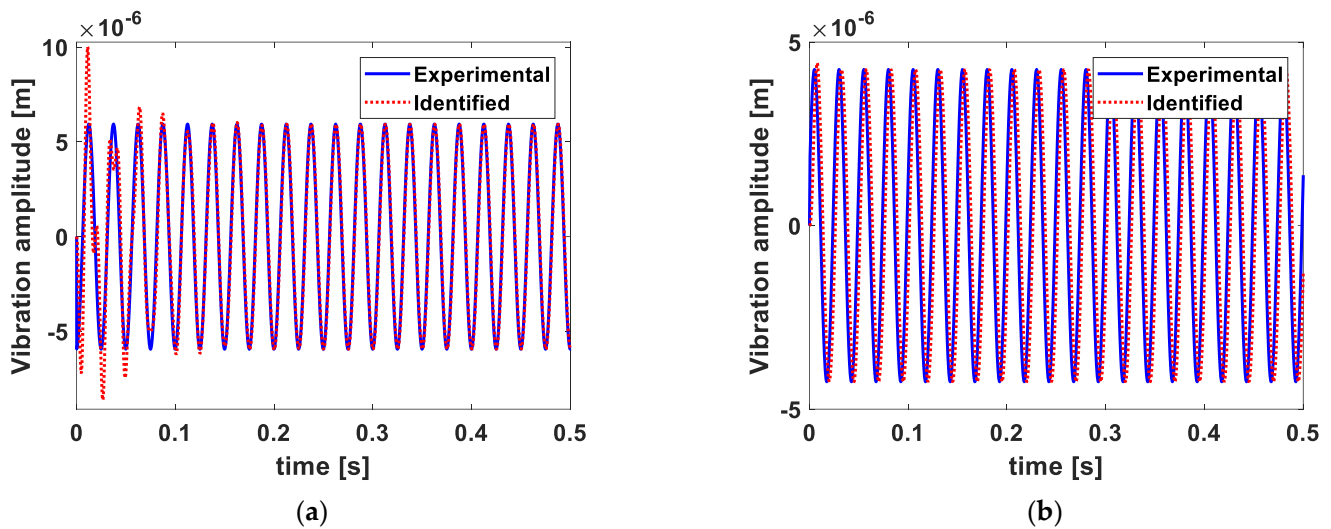
Figure 13. Rotor vibration response at 2400 rpm: experimental (blue line) and identified (red dots) parameters in the (**a**) X direction and (**b**) Z direction.

On the other hand, the rotor dynamic parameters identified by AI at different rotor speeds are presented in Table 6. Similar results to those depicted in Figure 13 were observed by comparing the vibration response that was experimentally obtained with that numerically obtained using the rotor dynamic parameters presented in Table 6. A vibration amplitude Bode Diagram was plotted from the vibration response amplitudes numerically obtained at each rotor speed for the speed interval of $0 \leq \text{rpm} \leq 6000$.

Table 6. Dynamic coefficients identified by AI compared with genetic algorithm GA.

Speed (rpm)	k_{xx}		k_{zz}		c_{xx}		c_{zz}	
	AI	GA	AI	GA	AI	GA	AI	GA
600	1.86×10^5	1.98×10^5	4.52×10^5	1.84×10^5	1.24×10^3	1.48×10^2	1.51×10^4	1.45×10^4
1200	1.80×10^5	2.18×10^5	8.27×10^5	9.69×10^5	1.13×10^3	3.45×10^1	3.74×10^3	2.55×10^2
2400	5.14×10^5	5.19×10^5	6.92×10^5	6.03×10^5	9.32×10^1	5.20×10^2	9.29×10^2	3.15×10^2
3000	8.87×10^5	1.38×10^6	9.07×10^5	1.58×10^6	1.02×10^3	6.00×10^2	1.53×10^3	1.25×10^1
4200	2.99×10^5	9.78×10^5	3.67×10^5	7.93×10^5	8.45×10^2	6.76×10^2	1.10×10^3	8.90×10^2
4800	3.58×10^5	1.43×10^4	5.02×10^5	1.01×10^4	1.08×10^3	9.30×10^2	8.40×10^2	9.07×10^2
5040	5.37×10^5	2.08×10^5	6.85×10^5	6.35×10^5	6.93×10^2	7.76×10^2	8.03×10^2	9.44×10^2
6000	1.65×10^6	1.46×10^6	2.14×10^6	1.94×10^6	6.05×10^2	9.30×10^3	4.58×10^2	9.84×10^3

Stiffness (N/m) − damping (Ns/m).

The comparison between the vibration responses numerically and experimentally obtained for the rotor speed interval of $0 \leq \text{rpm} \leq 6000$ is depicted in Figure 14a,b, which correspond to an amplitude Bode Diagram along the x and z directions, respectively, with a bearing pressure of 10 psi.

It can be observed in Figure 14a,b that the rotor vibration behavior numerically obtained using the rotor dynamic coefficients identified by AI at different rotor speeds is quite like that experimentally obtained, with the highest difference in the vibration amplitude response close to resonance (4500–5000 rpm), such as was observed in the numerical simulation depicted in Figure 3.

The behavior of the identified rotor dynamic coefficients as a function of the angular speed of the rotor is depicted in Figure 15.

To validate the rotor dynamic coefficients obtained by AI, the rotor dynamic system response was obtained at the speeds presented in Table 4; in this case, the rotor dynamic coefficients were obtained by using a Genetic Algorithm (GA) [31]. As mentioned previously in the manuscript, the identifier of the proposed direct dynamic coefficients only needs the response of the system due to the unbalance in order to identify the coefficients; for this reason a methodology was selected that, like the proposed identifier, would need only the response of the system to be able to identify the dynamic parameters of the bearing and that could be implemented in a practical way. For this reason,

a Genetic Algorithm was used that is inspired by genetics and natural selection [31] and only uses the response to the unbalance of the system to establish an objective function, thus being able to estimate the dynamic coefficients of the bearing. The comparison between the vibration response numerically obtained using the rotor dynamic coefficients obtained through GA and that experimentally obtained is depicted in Figure 16a,b.
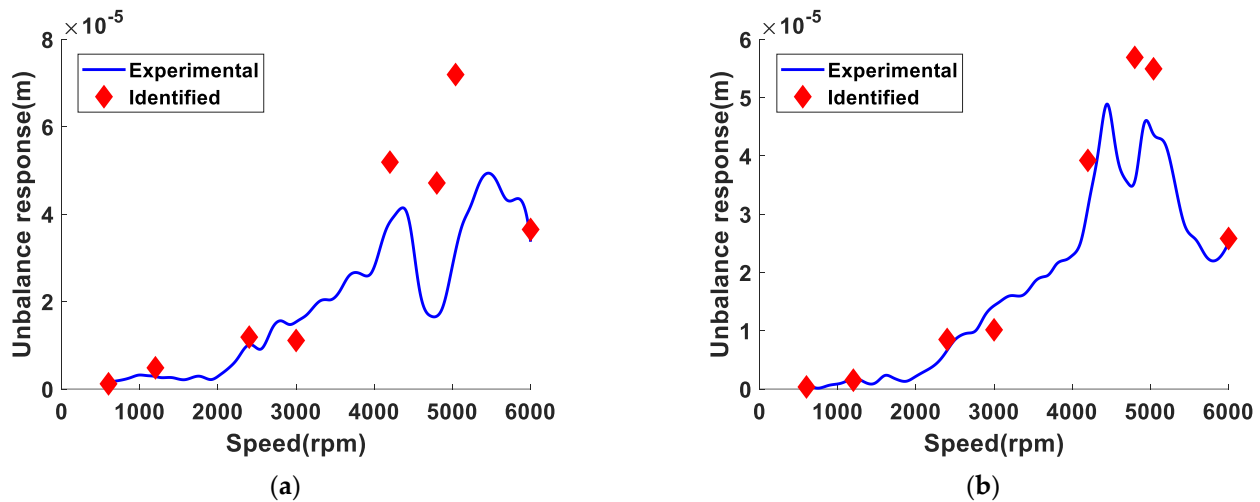

(**a**)　　　　　　　　　　　　　　　　　　　　　　　　　　(**b**)

Figure 14. Numerical and experimental Bode Diagram, node 11. (**a**) *X* direction and (**b**) *Z* direction.
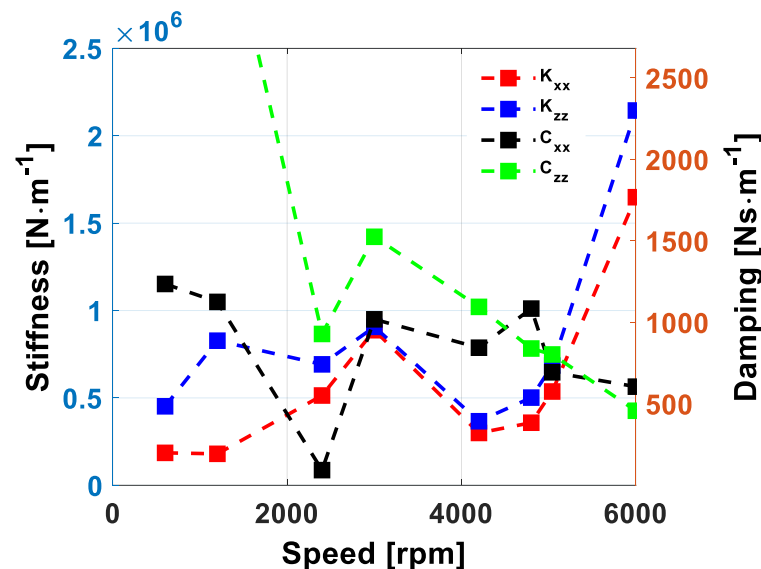

Figure 15. Rotor dynamic coefficients identified at different speeds (AI).

It can be observed in Figure 16a,b that the rotor vibration behavior numerically obtained using the rotor dynamic coefficients identified through GA at the different rotor speeds is quite similar to that experimentally obtained, with the highest amplitude response difference close to resonance (4500–5000 rpm). Likewise, the comparison among the vibration response experimentally obtained, the vibration response obtained through GA, and the vibration response obtained by the methodology proposed in this work using AI is depicted in Figure 17a,b.

It is possible to observe in Figure 17 that the vibration response calculated using the rotor dynamic coefficients obtained by GA exhibits similar behavior to that obtained using the rotor dynamic coefficients identified by AI. It can be also noted that, despite GA being a powerful tool, the identification of the rotor dynamic coefficients still lacks accuracy close to rotor resonance.

The behavior of the vibration response numerically obtained using the rotor dynamic coefficients identified by using the methodology proposed in the present work (AI) provides certainty on the veracity of the identified parameters; due to this, it was possible to reproduce the dynamics of the rotor–pressurized bearing when the pressure was at 10 psi, as depicted in Figures 13 and 17.
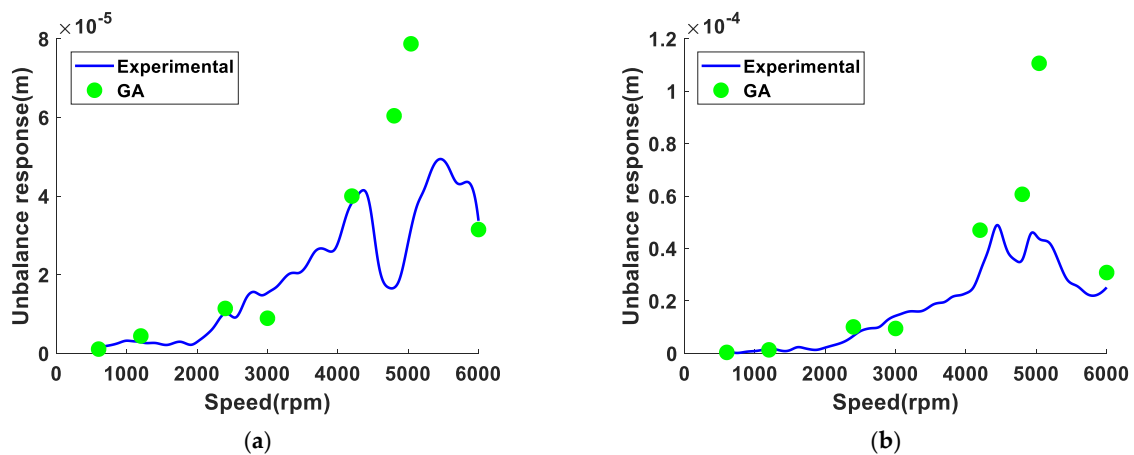
Figure 16. Experimental and numerical Bode Diagram using the rotor dynamic coefficients obtained by GA, node 11. (**a**) *X* direction and (**b**) *Z* direction.
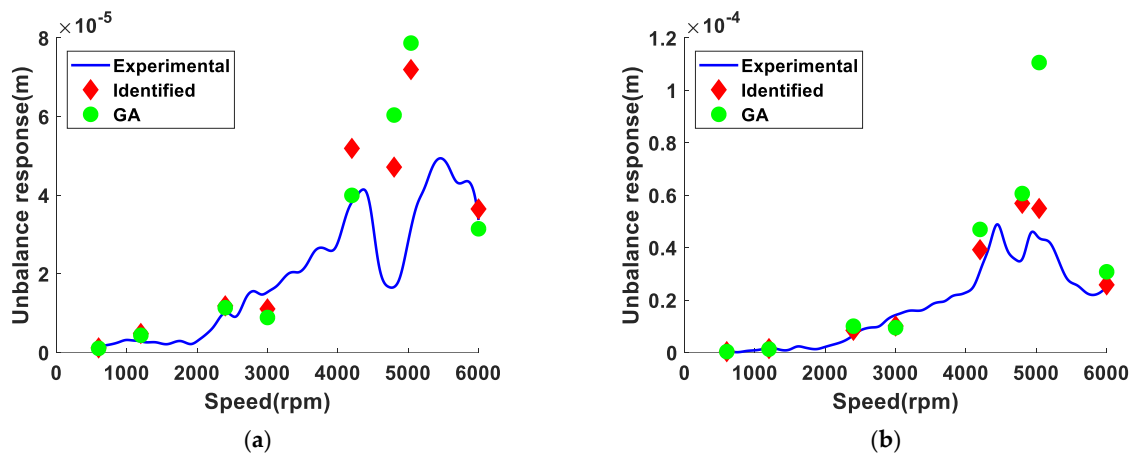

Figure 17. Experimental and numerical Bode Diagram using the rotor dynamic coefficients obtained by GA and AI, node 11. (**a**) *X* direction and (**b**) *Z* direction.

4. Discussion

Different simulations were carried out to test the functioning of the proposed algebraic identifier of rotodynamic coefficients. In the numerical simulation, the vibration response used by the identifier is obtained from the multiple-degrees-of-freedom model of Equation (3). It is important to highlight that the proposed identifier only uses the lateral displacements of a single node to identify the coefficients; in this case, it was node 11. This is a great advantage since other identifiers based on a more complex model need the entire displacement vector, i.e., the lateral vibration and the slope nodes of the node which you want to identify and of two adjacent nodes [23,24]. This is complex to achieve in the experimental part: First, the nodal slopes cannot be measured directly; it is best to approximate them with the lateral displacements. Second, instrumenting is complex since ten sensors would be used just to obtain the necessary displacements to identify the coefficients, which is a disadvantage. Meanwhile, the proposed identifier requires only two sensors (see Figure 10) to acquire the necessary displacements to identify the rotodynamic coefficients in an acceptable manner. This pair of sensors is placed in the position of the support to be identified (node 11).

It is important to highlight that when identifying the rotodynamic coefficients based solely on the unbalance response, there is an ill-conditioned matrix problem, which increases the algorithm complexity and decreases the precision of the identification results. It must be remembered that this algebraic identification methodology results in a system of equations (Equation (23)) where the matrix $A(t)$ and $P(t)$ change as a function of time; for this reason, the condition number of said matrices also changes. The condition number of a matrix is used to quantify its level of ill conditioning. If the condition number is close to 1, the matrix is said to be well conditioned. If the condition number is significantly greater than 1, the matrix is said to be ill conditioned. In this case, small

variations in the data can produce large variations in the results. It is common to find ill-conditioned matrices in inverse problems, as is the case of the proposed identifier. However, with the identified parameters, it is possible to reproduce the dynamics of the system with very few differences (see Figures 13 and 14). Taking this into account, an identifier of the direct rotodynamic coefficients was proposed with a reduced model, which has systems of 2×2 equations (see Equation (18)), resulting in a more stable identifier compared with more complex models with 8×8 matrices and with a higher condition number.

Figure 18 shows the condition number of the matrices A (blue line) and P (red line), calculated with the experimental measurements of the displacements at a speed of 2400 rpm. It can be seen how the number of conditions tends to decrease after a short time and ends up oscillating between a large range of values. Even with this behavior, the proposed algebraic identifier fulfills its function of estimating the rotodynamic parameters, and with these identified parameters, it is possible to reproduce the dynamics of the rotodynamic system acceptably (see Figure 14). It can be seen in Figure 14 that the greatest difference between the experimental responses and the numerical one obtained with the identified dynamic coefficients is found at speeds close to resonance (4500–5000 rpm), as observed in the numerical simulation represented in Figure 3, where both models are compared. These differences are mainly because Equation (12) is taken as the basis for the development of the proposed identifier Equation (17) in a simplified model of two degrees of freedom, while in the experimental part, there is a rotor-bearing system with multiple degrees of freedom. This is a limitation of the identifier. Another limitation is that the developed identifier only identifies the direct coefficients and misses the crossed coefficients, which are essential to more accurately reproduce the dynamics of the system. It is very important to monitor the crossed coefficients since it is known that certain values can cause instabilities in the rotor-bearing system.
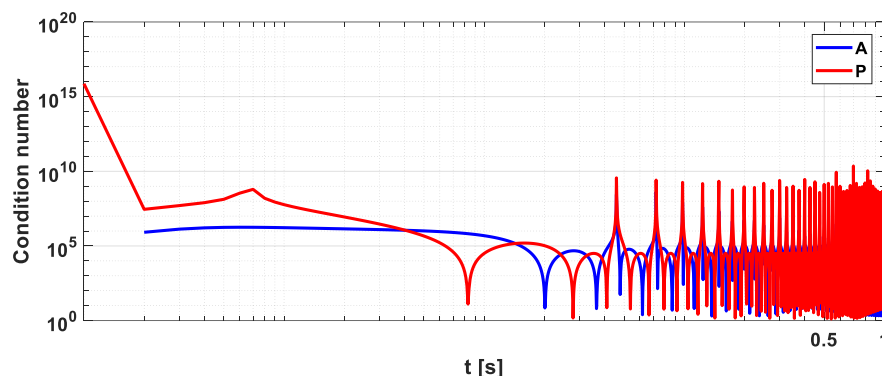

Figure 18. Condition number of matrices A and P with experimental data at a speed of 2400 rpm.

5. Conclusions

This research focuses on the determination of the direct dynamic coefficients of a pressurized bearing in a rotor-bearing system. An online identifier was developed based on the algebraic technique aimed at determining the magnitude of both the stiffness (k_{xx}, k_{zz}) and damping (c_{xx}, c_{zz}) coefficients of the rotor dynamic system. The proposed identifier only requires the rotor vibration response at a constant frequency as input data. The numerical and experimental results show that the proposed methodology is reliable since the identification of the rotor dynamic parameters is achieved in less than 0.2 s. The experimental rotor vibration response at constant frequency was used as input data to validate the accuracy of the proposed identifier. The vibration response was acquired between 600 and 6000 rpm, passing through the first bending critical speed of the rotor with a pressure of 10 psi. From the identified rotor dynamic coefficients, the rotor vibration response was obtained numerically and then compared to the amplitude Bode Diagram at the same pressure. The results show a negligible error of the bearing dynamic coefficients' identified parameters with respect to those of the experimental bearing since it was possible to reproduce the experimental rotor-bearing system dynamics. It is important to highlight that the developed identifier only identifies the direct coefficients and misses the crossed coefficients which are essential to be able to more accurately reproduce the dynamics of the system. It is very important to monitor the crossed coefficients since it is known that certain values can cause instabilities in the rotor-bearing system. The algebraic identifier of the direct rotodynamic coefficients of a pressurized bearing can also be used in other types of bearings. In this case, it was used for a pressurized bearing, considering constant speed and constant pressure; this means that it can be used to identify the parameters' conventional bearings,

where their rotodynamic coefficients are considered constant, or magnetic bearings, where their properties change depending on the current supplied to the support. This is possible because in the mathematical model used for the development of the identifiers, only the effects of stiffness and damping attributable to the support are considered, without considering their nature.

The main advantage of the present methodology is its easy application to active control systems since the determination of the rotor dynamic coefficients of rotating machines as a function of the operating conditions in-situ is the basic information used in the design of vibration control systems.

Author Contributions: Conceptualization, S.J.L.-D., J.C.-O. and A.B.-O.; methodology, S.J.L.-D., A.A.-P. and D.P.-V.; software, S.J.L.-D., J.G.M.-L. and L.A.B.-T.; validation, S.J.L.-D. and J.C.-O.; formal analysis, S.J.L.-D., D.P.-V. and L.A.B.-T.; investigation, S.J.L.-D., J.G.M.-L. and A.A.-P.; resources, S.J.L.-D., J.C.-O. and A.B.-O.; data curation, S.J.L.-D., L.A.B.-T. and J.C.-O.; writing—original draft preparation, S.J.L.-D., D.P.-V. and A.A.-P.; writing—review and editing, S.J.L.-D., A.B.-O. and A.A.-P.; visualization, S.J.L.-D., J.G.M.-L. and L.A.B.-T.; supervision, S.J.L.-D., J.C.-O. and A.B.-O.; project administration, S.J.L.-D., J.G.M.-L. and D.P.-V.; funding acquisition, S.J.L.-D., J.C.-O. and A.B.-O. All authors have read and agreed to the published version of the manuscript.

Data Availability Statement: The datasets generated and supporting the findings in the article are obtainable from the corresponding author upon reasonable request.

Conflicts of Interest: The authors declare no conflict of interest.

Nomenclature

k_{xx}, k_{zz}	Direct dynamic coefficients of stiffness	k_r	Stiffness of the rotor
k_{xz}, k_{zx}	Cross-coupled dynamic coefficients of stiffness	$\ddot{\phi}$	Angular acceleration
c_{xx}, c_{zz}	Direct dynamic coefficients of damping	E	Modulus of elasticity
c_{xz}, c_{zx}	Cross-coupled dynamic coefficients of damping	ρ	Density
u_i, w_i	Lateral displacements	v	Poisson ratio
ψ_i, θ_i	Angular displacements	r_s	Radius of shaft
$\{\delta\}$	Vector containing the nodal displacements;	L_e	Element length
m_u, d, α	The mass, eccentricity, and angular position of the unbalance, respectively	e_D	Disk thickness
$[M]$	The global mass matrix of the system	r_{iD}	Inner radius of the disk
$[C(\Omega)]$	The global damping matrix	r_{eD}	Outer radius of the disk
$\left(\dot{\phi}[C_2]\right)$	The gyroscopic effects as a function of the angular speed	t	Time
$[C_1]$	Damping attributable to the supports	$A(t)$, $P(t)$	Algebraic identifier coefficient arrays
$\left[K\left(\ddot{\phi}\right)\right]$	The global stiffness matrix	$B_1(t)$, $B_2(t)$	Vectors of independent terms of the algebraic identifier
$[K_1]$	The stiffness attributable to the supports	Θ_1, Θ_2	The dynamic parameter vectors to identify
$[K_2]$	The stiffness attributable to the rotor	D_j	Diameter of journal
$\ddot{\phi}[K_3]$	Stiffness matrix as a function of the angular acceleration of the rotor	L_j	Length of journal
$\left\{F_{u(1)}(\phi)\right\}$; $\left\{F_{u(2)}(\phi)\right\}$	The vectors of the centrifugal force components generated by the unbalance mass	L_j/D_j	Length-to-diameter ratio
$R_0(XZY)$	The inertial frame	c_r	Radial clearance of journal bearing
Ω	The speed of rotation	d_p	Fluid injection port diameter
L	Length of shaft	P_1, P_2, P_3, P_4	Fluid injection ports
l_1	Unbalance mass location		
l_2	Journal-bearing location		
q_1, q_2	Generalized independent coordinates		
f	Modal shape function		
E_k	The kinetic energy		
U	The strain energy		
δW	The virtual work		

Appendix A

Kinetic energy, strain energy, and the virtual work for the elements of the rotor-bearing system [29].

Appendix A.1

The kinetic energy of the disk T_D

$$T_D = \frac{1}{2}\left[M_D f^2(l_1) + I_{Dx}g^2(l_1)\right]\left(\dot{q}_1^2 + \dot{q}_2^2\right) - I_{Dy}\Omega g^2(l_1)\dot{q}_1 q_2 \tag{A1}$$

M_D = Mass of the disk
I_{Dx} = Moment of inertia around axis X
I_{Dy} = Moment of inertia around axis Y.

Appendix A.2

The kinetic energy of the shaft T_S

$$T_S = \frac{1}{2}\left[\rho S \int_0^L f^2(y)dy + \rho I \int_0^L g^2(y)dy\right]\left(\dot{q}_1^2 + \dot{q}_2^2\right) - 2\rho I \Omega \int_0^L g^2(y)dy\,\dot{q}_1 q_2 \tag{A2}$$

ρ = Density of the shaft
S = Cross-section
I = Moment of inertia

Appendix A.3

The kinetic energy of the disk-shaft assembly E_k

$$E_k = T_D + T_S \tag{A3}$$

$$E_k = \frac{1}{2}\left[M_D f^2(l_1) + I_{Dx}g^2(l_1) + \rho S \int_0^L f^2(y)dy + \rho I \int_0^L g^2(y)dy\right]\left(\dot{q}_1^2 + \dot{q}_2^2\right) - \Omega\left[I_{Dy}g^2(l_1) + 2\rho I \int_0^L g^2(y)dy\right]\dot{q}_1 q_2 \tag{A4}$$

Equation (A4) can be written in a more compact form as:

$$E_k = \frac{1}{2}m\left(\dot{q}_1^2 + \dot{q}_2^2\right) - \Omega a \dot{q}_1 q_2 \tag{A5}$$

where:

$$m = M_D f^2(l_1) + I_{Dx}g^2(l_1) + \rho S \int_0^L f^2(y)dy + \rho I \int_0^L g^2(y)dy$$
$$a = I_{Dy}g^2(l_1) + 2\rho I \int_0^L g^2(y)dy$$

Appendix A.4

The strain energy of the shaft U_S.
If the axial force is null, then the strain energy of the shaft is:

$$U_S = \frac{EI}{2}\int_0^L h^2(y)dy\left(q_1^2 + q_2^2\right) \tag{A6}$$

E = Elasticity module
Equation (A6) can be written in a more compact form as:

$$U_S = \frac{1}{2}k\left(q_1^2 + q_2^2\right) \tag{A7}$$

where:

$$k = EI\int_0^L h^2(y)dy$$

Appendix A.5

The bearing virtual work δW.

The virtual work done by the forces due to the bearing acting on the shaft is given by:

$$
\begin{aligned}
\delta W = &-k_{xx}f^2(l_2)q_1\delta q_1 - k_{xz}f^2(l_2)q_2\delta q_1 - k_{zz}f^2(l_2)q_2\delta q_2 - k_{zx}f^2(l_2)q_1\delta q_2 \\
&-c_{xx}f^2(l_2)\dot{q}_1\delta q_1 - c_{xz}f^2(l_2)\dot{q}_2\delta q_1 - c_{zz}f^2(l_2)\dot{q}_2\delta q_2 \\
&-c_{zx}f^2(l_2)\dot{q}_1\delta q_2
\end{aligned}
\tag{A8}
$$

as

$$
\delta W = Fq_1\delta q_1 + Fq_2\delta q_1
\tag{A9}
$$

Fq_1 and Fq_2 denote the generalized force acting on the shaft.

Appendix A.6

The kinetic energy of the unbalance mass T_u.
The kinetic energy of the unbalance mass is given by:

$$
T_u = m_u df(l_1)\Omega\big[\dot{q}_1\cos(\Omega t + \alpha) - \dot{q}_2\sin(\Omega t + \alpha)\big]
\tag{A10}
$$

m_u = unbalance mass
d = distance from the geometric center of the shaft to mass unbalance.

References

1. Lund, J.W. *Self-Excited, Stationary Whirl Orbits of a Journal in a Sleeve Bearing*; Rensselaer Polytechnic Institute: Troy, NY, USA, 1966.
2. Vance, J.M. *Rotordynamics of Turbomachinery*; John Wiley & Sons: New York, NY, USA, 1988; ISBN 0471802581.
3. Dimarogonas, A. *Vibration for Engineers*, 2nd ed.; Prentice Hall: Hoboken, NJ, USA, 1996; ISBN 0134562291.
4. Mao, W.; Li, J.; Huang, Z.; Liu, J. Bearing dynamic parameters identification for a sliding bearing-rotor system with uncertainty. *Inverse Probl. Sci. Eng.* **2017**, *26*, 1094–1108. [CrossRef]
5. Chen, C.; Jing, J.; Cong, J.; Dai, Z. Identification of dynamic coefficients in circular journal bearings from unbalance response and complementary equations. *Proc. Inst. Mech. Eng. Part J J. Eng. Tribol.* **2018**, *233*, 1016–1028. [CrossRef]
6. Zhao, K.; Hu, J.; Shao, H.; Hu, J. Federated multi-source domain adversarial adaptation framework for machinery fault diagnosis with data privacy. *Reliab. Eng. Syst. Saf.* **2023**, *236*, 109246. [CrossRef]
7. Puerto-Santana, C.; Ocampo-Martinez, C.; Diaz-Rozo, J. Mechanical rotor unbalance monitoring based on system identification and signal processing approaches. *J. Sound Vib.* **2022**, *541*, 117313. [CrossRef]
8. Zhao, K.; Jia, F.; Shao, H. A novel conditional weighting transfer Wasserstein auto-encoder for rolling bearing fault diagnosis with multi-source domains. *Knowl. Based Syst.* **2023**, *262*, 110203. [CrossRef]
9. Shrivastava, A.; Mohanty, A.R. Identification of unbalance in a rotor system using a joint input-state estimation technique. *J. Sound Vib.* **2018**, *442*, 414–427. [CrossRef]
10. Chen, Y.; Yang, R.; Sugita, N.; Mao, J.; Shinshi, T. Identification of Bearing Dynamic Parameters and Unbalanced Forces in a Flexible Rotor System Supported by Oil-Film Bearings and Active Magnetic Devices. *Actuators* **2021**, *10*, 216. [CrossRef]
11. Ocampo, J.C.; Wing, E.S.G.; Moroyoqui, F.J.R.; Pliego, A.A.; Ortega, A.B.; Mayén, J. A novel methodology for the angular position identification of the unbalance force on asymmetric rotors by response polar plot analysis. *Mech. Syst. Signal Process.* **2017**, *95*, 172–186. [CrossRef]
12. Yao, J.; Liu, L.; Yang, F.; Scarpa, F.; Gao, J. Identification and optimization of unbalance parameters in rotor-bearing systems. *J. Sound Vib.* **2018**, *431*, 54–69. [CrossRef]
13. Li, L.; Luo, Z.; He, F.; Sun, K.; Yan, X. Experimental and numerical investigations on an unbalance identification method for full-size rotor system based on scaled model. *J. Sound Vib.* **2022**, *527*, 116868. [CrossRef]
14. Wang, A.; Yao, W.; He, K.; Meng, G.; Cheng, X.; Yang, J. Analytical Modelling and Numerical Experiment for Simultaneous Identification of Unbalance and Rolling-Bearing Coefficients of the Continous Single-Disc and Single-Span Ro-tor-Bearing System with Rayleigh Beam Model. *Mech. Syst. Signal Process.* **2019**, *116*, 322–346. [CrossRef]
15. On, S.Y.; Kim, Y.S.; You, J.I.; Lim, J.W.; Kim, S.S. Dynamic characteristics of composite tilting pad journal bearing for turbine/generator applications. *Compos. Struct.* **2018**, *201*, 747–759. [CrossRef]
16. Xu, Y.; Zhou, J.; Di, L.; Zhao, C. Active magnetic bearings dynamic parameters identification from experimental rotor unbalance response. *Mech. Syst. Signal Process.* **2017**, *83*, 228–240. [CrossRef]
17. Xu, Y.; Zhou, J.; Lin, Z.; Jin, C. Identification of dynamic parameters of active magnetic bearings in a flexible rotor system considering residual unbalances. *Mechatronics* **2018**, *49*, 46–55. [CrossRef]
18. Varnusfaderani, M.A.; Parizi, M.I.; Hemmatian, M.; Ohadi, A. Experimental parameters identification of a flexible rotor system equipped with smart magneto-rheological bearing. *Mechatronics* **2022**, *87*, 102880. [CrossRef]
19. Guenat, E.; Schiffmann, J. Dynamic force coefficients identification on air-lubricated herringbone grooved journal bearing. *Mech. Syst. Signal Process.* **2019**, *136*, 106498. [CrossRef]
20. Sadiq, M.I.; Ghopa, W.A.W.; Nuawi, M.Z.; Rasani, M.R.; Khamis, N.K.; Abu Mansor, M.R. Investigation of stiffness and damping coefficients in fluid film bearing with bio-oils and mineral-based oil. *Energy Rep.* **2022**, *8* (Suppl. S9), 419–429. [CrossRef]

21. Sayed, H.; El-Sayed, T. Nonlinear dynamics and bifurcation analysis of journal bearings based on second order stiffness and damping coefficients. *Int. J. Non-Linear Mech.* **2022**, *142*, 103972. [CrossRef]
22. Fliess, M.; Sira–Ramírez, H. An algebraic framework for linear identification. *ESAIM Control Optim. Calc. Var.* **2003**, *9*, 151–168. [CrossRef]
23. Mendoza-Larios, J.G.; Barredo, E.; Arias-Montiel, M.; Baltazar-Tadeo, L.A.; Landa-Damas, S.J.; Tapia-Herrera, R.; Colín-Ocampo, J. An Algebraic Approach for Identification of Rotordynamic Parameters in Bearings with Linearized Force Coefficients. *Mathematics* **2021**, *9*, 2747. [CrossRef]
24. Baltazar-Tadeo, L.A.; Colín-Ocampo, J.; Mendoza-Larios, J.G.; Abúndez-Pliego, A.; Nango-Blanco, M.; Blanco-Ortega, A.; Landa-Damas, S.J. An Integrated Balancing Method for Asymmetric Rotor-Bearing Systems: Algebraic Identification, Modal Balancing, and Active Balancing Disks. *J. Vib. Eng. Technol.* **2022**, *11*, 619–645. [CrossRef]
25. Nango, B.M. Identificación Algebraica en Línea de Parámetros para el Balanceo de rotores Asimétricos. Master's Thesis, Tesis de Maestría en Ciencias en Ingeniería Mecánica, CENIDET, Tecnológico Nacional de México, Cuernavaca, Mexico, 2015.
26. Carvajal, F.B.; Navarro, G.S.; Ramíres, H.S.; Ortega, A.B. Active Vibration Control Using On-Line Algebraic Identification and Sliding Modes. *Comput. Y Sist.* **2010**, *13*, 313–330.
27. Arias, M.M.; Carvajal, F.B.; Navarro, G.S. On-Line Algebric Identification of Eccentricity Parameters in Active Rotor-Bearing Systems. *Int. J. Mech. Sci.* **2014**, *85*, 152–159. [CrossRef]
28. Mendoza Larios, J.G.; Colín Ocampo, J.; Blanco Ortega, A.; Abúndez Pliego, A.; Gutiérez Wing, E.S. Balanceo Automatico de un Sistema Rotor-Cojinete: Identificador Algebraico en Línea del Desbalance Para un Sistema Rotodinámico (Automatic Balancing of a Rotor-Bearing On-Line Algebraic Identifier for a Rotordynamic Balancing System). *Rev. Iberoam. Autom. Inform. Ind. RIAI* **2016**, *13*, 281–292. [CrossRef]
29. Lalanne, M.; Ferraris, G. *Rotordynamics Prediction in Engineering*; John Wiley & Sons Ltd.: Hoboken, NJ, USA, 1990; ISBN 0471926337.
30. Kim, Y.-H.; Yang, B.-S.; Tan, A.C.C. Bearing parameter identification of rotor–bearing system using clustering-based hybrid evolutionary algorithm. *Struct. Multidiscip. Optim.* **2006**, *33*, 493–506. [CrossRef]
31. Shiffman, D. *The Nature of Code: Simulating Natural Systems with Processing*, 1st ed.; 2012. Available online: https://freecomputerbooks.com/The-Nature-of-Code-Simulating-Natural-Systems-with-Processing.html (accessed on 1 June 2023).